UiT
THE ARCTIC UNIVERSITY OF NORWAY

FACULTY OF SCIENCE AND TECHNOLOGY

Department of Geology

Shallow and Deep Seismic Amplitude Anomalies Indicate Times of Fluid Accumulation and Tectonic Activity in the Barents Sea

—

Magnus Pedersen

EOM-3901 Master thesis in Energy, Climate and Environment
June, 2016

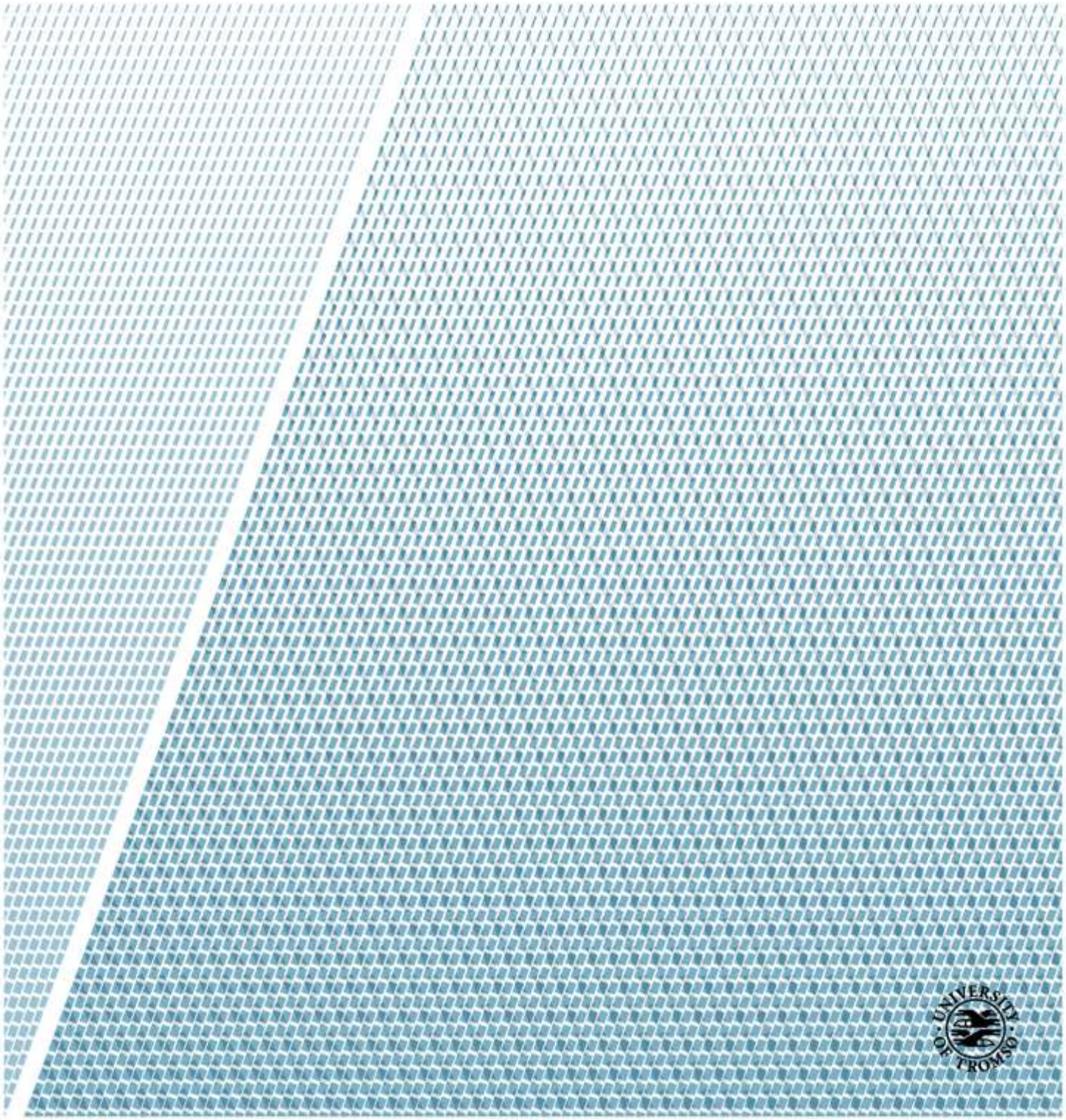

Abstract.

This master thesis studied the 3D-seismic dataset ST0825 located in the southwest Barents Sea. Aiming to map seismic anomalies and faults above and below the Upper Regional Unconformity (URU).

The survey partly covers four different structural elements: Finnmark Platform, Tromsø Finnmark Fault Complex, Hammerfest Basin and Ringvassøy Loppa Fault Complex, south to north respectively. These areas are all affected by the tectonic activity from the Caledonian orogeny to lastly the creation of the North Atlantic Ocean. Making the study area complex with different faulting orientations and activity timing.

The lithostratigraphy of the survey were mapped with the help of wellbore 7119/12-1, 7119/12-4 and existing publications. The different faults are mapped and categorized into First – Third class. Also, the seismic anomalies are mapped, interpret and discussed.

In the survey, there are indications of migration hydrocarbon using mainly faults as migration pathways. There were also mapped a polygonal fault system, the same as Ostanin et al., (2012) mapped in the Hammerfest Basin.

There were not found any indications that there have been tectonic activity post-URU, but there were indications that there has been fluid flow activity after its deposition with pockmarks mapped on the seafloor.

Acknowledgement

Med dette starter en ny epoke i mitt liv. Det er veldig spennende, samtidig som veldig skummelt, virkelig skrekkblandet fryd! Men etter disse seks årene takker jeg for meg som siv.ing student på EKM. De siste årene har lært meg mye, både faglig og personlig. Takk for alle festene, de seine kveldene og kameraderiet. Studentlivet har vært flott og jeg har fått venner for livet.

Tusen takk til Universitetet i Tromsø, spesielt for utvekslingsåret.

Tusen takk til min veileder Jürgen Mienert, din tålmodighet og veiledning har vært til stor hjelp. Det har vært en ære.

Og ikke minst, takk for all støtten fra alle sammen!

Det har vært til stor hjelp.

In Memoriam Thomas ‘Timber’ Nicholaysen

«Uten mat og drikke, duger helten ikke.»

Norwegian Proverb

Table of Contents

Abbreviations used.

API = American Petroleum Institute (3.3.1 Gamma Ray.)

FP = Finnmark Platform.

HB = Hammerfest Basin

mbsf = meter below seafloor.

mbsl = meter below sea level

NPD = Norwegian Petroleum Directorate.

RLFC = Ringvassøy-Loppa Fault Complex

TFFC = Tromsø-Finnmark Fault Complex.

TVD = True Vertical Depth, m. I.e. the vertical distance from a surface point.

TWT = Two Way Travel time, usually in ms.

URU = Upper regional unconformity.

1 Introduction.

1.1 Objectives.

The main goal is to map seismic anomalies and fault systems beneath the upper regional unconformity (URU) and systems that penetrate the URU.

Aims are to better understand tectonic active periods controlling the occurrence and development of large and small-scale fault systems, fluid accumulation inferred from seismic anomalies and their relationship to the structural development and denudation history of the Barents Sea.

Tectonic activity after ice sheet retreat and unloading is of particular interest. Secondary goals include the determination and analysis of fluid escape routes, i.e. through URU.

Much of the work will be interpreting the distribution of deep and shallow faults, erosional horizons, location of seismic amplitudes, of URU and the thickness above. It allows to shed more light on the erosional environment and tectonic development in a formerly ice-sheet dominated region.

Visualizing the vertical and lateral distribution of faults that penetrate URU and significant fluid escape routes using 3D and 2D seismic data including boreholes for the stratigraphy calibration will be the main task.

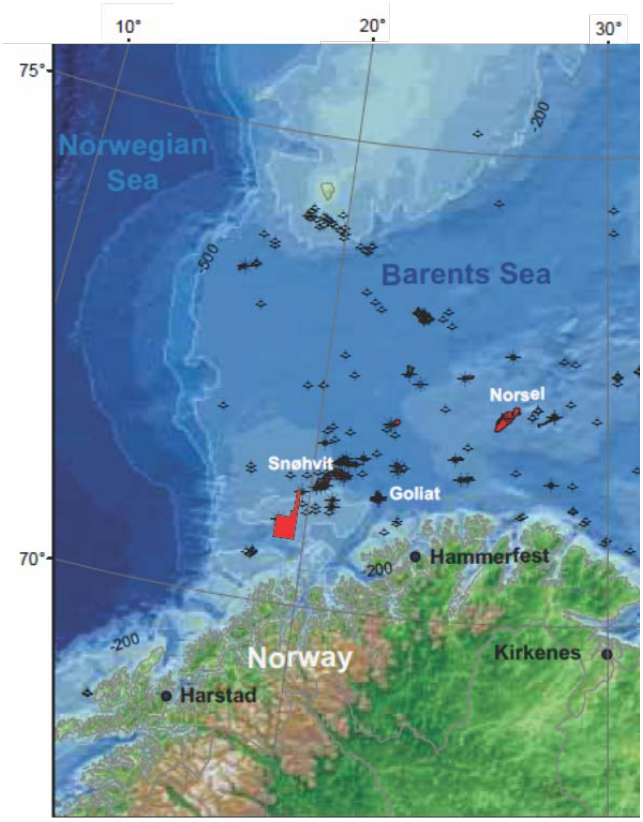

1.2 Theory.

In this chapter the theoretical foundations is laid. Here the reader will be able to learn about the different features, which makes up the interpretation work and its theoretical background and will go through seismic basics, the physical laws, which the interpreted features are based on and the interpretation features themselves.

1.2.1 Seismic basics.

To investigate seafloor and sub-seafloor features different types of acoustic technologies are used: high frequency mulitibeam echo sounders for mapping the seafloor and a low frequency air guns generating seismic waves, i.e. compressional waves for 2D and/or 3D reflection seismic studies of the sub-seafloor (Wille, 2005). The speed of sound of compressional waves in the water column and beneath the seafloor allows to calculate distance and object size. However, the two-way travel time needs to be considered for any calculation and processing to determine both distance to target formations and their size, this covers the basics for reflection seismic studies.

1.2.1.1 Basic reflection seismic theory.

Two types of waves are emitted in a spherical motion from the shot-point, known as P- and S-waves. The data in this study stems from marine reflection seismics in the ocean and since no shear waves can be generated in fluids, there are no S-waves recorded. The reason for this is that S-waves are reliant on the rigidity modulus of the medium it travels through; and water's rigidity modulus is approximately zero (Burger et al., 2006). Hereby and onwards if the speed of sound or seismic waves are mentioned, only P-waves are to be considered.

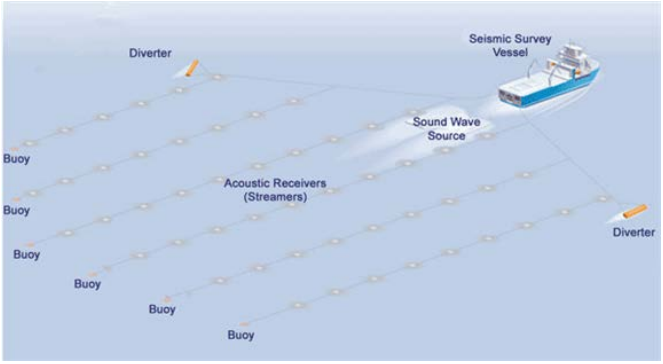

Fig. 1: Schematic sketch of marine seismic survey. A vessel tows a soundwave source and several lines of hydrophones. From (Fishsafe.eu)

A marine seismic survey consists of a seismic survey vessel, which tows a GI gun or gun array comprising the soundwave source and a hydrophone or hydrophone array comprising the streamers. There can be many parallel seismic lines, where a streamer cable with hydrophones can be up to 20 km long (Canty, 2014). A general schematic sketch for a marine seismic survey shows Fig. 1. A 3-D set-up, i.e. several streamers are being towed by the vessel provide a 3D view of the sub seafloor geology.

To interpret the sub-seafloor the soundwaves need to reflect or refract from a layer boundary within the sub seafloor. For exploration seismics it is the reflected wave, which are recorded by hydrophones within the streamer array (Burger et al., 2006).

As the wave travels through a layer medium some of its energy will be lost, because of the new secondary wavelets generation, this is Huygen's Principle (Fig. 2)(Burger et al., 2006)

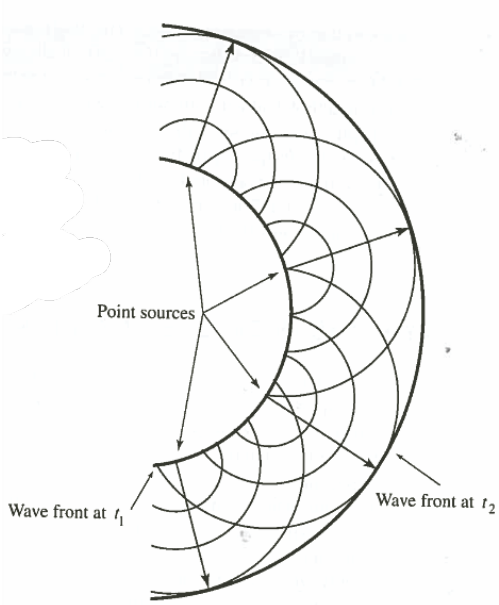

Fig. 2: Huygen's Principle illustrated. The point source indicate where the previous wavelet hit the border of a new medium generating new wavelets.

To be recorded, the amplitude of the reflected wave needs to be strong enough, i.e. above noise level in order to be recorded as a reflection event. Because of the spherical spreading the energy, i.e. the amplitude of the wave decreases, with the rate of Equation 1. (Fig. 2) (Burger et al., 2006). Eq. 1. states that the energy intensity (I) is reduced by the energy absorption of the medium (q) times the distance (r).

Equation 1: $$I = I_0 e^{-qr}$$

The amplitude of the reflected waves are calculated from equations Zoeppritz derived in 1919 (Burger et al., 2006). One of these equations allows to calculate the amplitude of the reflected wave (Burger et al., 2006). Given the porosity (ρ) and the velocity (ν) that the P-wave will have to travel through the layer Zoeppritz came up with the following equation to calculate the acoustic impedance, the product of material density x compressional wave velocity. If the difference between an upper and lower layer is significant, i.e. the reflection coefficient, a seismic reflector may be generated at the interface between layer 1. and 2., where R is the difference of the two layer's using density x velocity:

Equation 2: $$R = \frac{A_{rfl}}{A_i} = \frac{\rho_2 \nu_2 - \rho_1 \nu_1}{\rho_2 \nu_2 + \rho_1 \nu_1}$$

Equation 3: $$Z = \rho \; x \; \nu$$

This reflection coefficient (R) shows a value between 0 and 1. A reflected wave may be generated when the acoustic impedance change significantly between layer 2. and 1. However, as mentioned before, the reflected waves amplitude must be recognizable by the hydrophones in the streamer. If the reflection coefficient is too low the layer will not appear in the resulting reflection seismic profile as a reflector. The wave velocity through the medium may differ greatly if the pore space of the sediments/rocks are filled with gas or oil, e.g. different forms of hydrocarbons. Thus, reflection seismic methods are regularly used in hydrocarbon exploration worldwide.

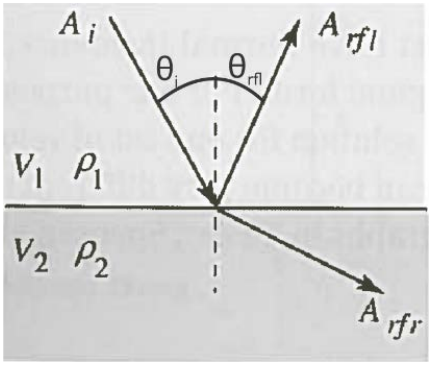

Fig. 3: Showing the quantities Zoeppritz used in his equation. An incoming wave with amplitude, A_i, reflects with one amplitude A_{rfl} and refracts with another amplitude A_{rfr}. Modified from (Burger, Sheehan et al., 2006)

1.2.1.2 Seismic resolution.

After the recording and processing of the data it is important to know the technical specification of a survey. By knowing the initial frequency and wavelength of the compressional wave, the shot point interval, and the hydrophone interval in the streamer, an interpreter may make some rough calculations to derive the seismic vertical and horizontal resolution. This can be important to know because it puts boundaries on the minimum detectable target size of structures and formations.

1.2.1.3 Compressional Wave velocity.

Compression-wave's, i.e. P-waves, velocity through a medium may vary greatly with the amount of gas present in the pore space of sediments. Because of this dependence on the amount of gas it can be clearly visible on, a well processed, seismic reflection profile. Fig. 4,

shows compressional wave's velocity (V_p) through a medium with gas where the most dramatic change occurs when the gas concentration goes from 0-8% saturation.

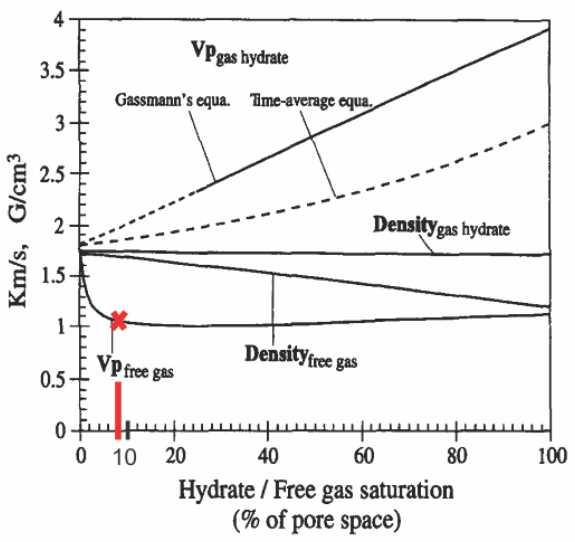

Fig. 4: Red cross indicate the ~8% mark of gas concentrations, higher values do not lead to a significant velocity increase. The y-axis shows velocity for the Vp and density. The x-axis indicate the percentage of hydrate gas in the medium. Modified from (Andreassen, Hart et al., 1997)

1.2.2 Basic Mechanics of Fluid Flow.

In the subsurface there are many kinds of fluid with different properties, e.g. mud, brine, hydrocarbons etc. (Andreassen, Nilssen et al., 2007; Berndt, 2005; Ligtenberg, 2005; Ligtenberg & Connolly, 2003; Watterson, Walsh et al., 2000). The understanding of the fluids and their movement and mechanics in general are of great importance to understand the subsurface, geological features on the seafloor, marine biological processes and the general composition of the oceans (Hovland & Judd, 1988). With the 3D – seismic and constantly improving computer technology it is possible to explore and investigate the subsurface as never before (Berndt, 2005).

In general, there are three laws of physics that the basic mechanics of fluid flow are based on. These laws are: Darcy's - and Fick's Law and the mechanisms of advective flow (Berndt, 2005).

1.2.2.1 Darcy's Law.

Darcy's Law is one of the most important laws in physics for studying fluid flow in porous and permeable sediments (Berndt, 2005; Vincent, Muthama et al., 2014). Darcy's law describe the fluid flow flux (q) through a permeable medium due to pressure differences (p). This fluid flux depends on the permeability of the medium (k) and the viscosity (μ) (Equation 4).

Equation 4: $$q = \frac{-k}{\mu} \nabla p$$

Note that Darcy's Law presume that the system have laminar flow through a bulk medium where hydraulic conductivity is valid (Berndt, 2005; Vincent et al., 2014).

1.2.2.2 Fick's Law of Diffusion.

The Fick's law of diffusion stat the rate of which a solution will be diffused, or rather the transportation of molecules which lead to this effect. If the process is in a porous media, e.g. sedimentary layer, Fick's Law is formulated as in Equation 5. (Krooss & Leythaeuser, 1996). Fick's law state that the diffusive flux (J) is equal to the effective diffusion (D_{Eff}) to the concentration gradient of the bulk volume concentration (C_{Bulk}) (Equation 5) (Krooss et al., 1996).

Equation 5: $$J = -D_{eff} \cdot \nabla C_{Bulk}$$

Where Darcy's Law state that fluid movement is due to pressure differences, Fick's Law state that molecules within the fluid moves due to concentration differences. I.e. pore-fluid in a medium with non-uniform concentration will have molecular movement from high- to low concentration area.

1.2.2.3 Advective Flow.

Advection is the movement, or rather transport, of properties or contents by fluids due to the fluid's bulk motion, induced by pressure and density gradients (Alcaraz, García-Gil et al., 2016; Moore & Wilson, 2005). E.g. transportation of heat, pollution, suspended material etc. In geology, it refers to movement of fluids through high permeability zones, e.g. fractured rocks, hydrothermal vents, and is used when for example discussing heat flow (Alcaraz et al., 2016; Moore et al., 2005)

1.2.3 Seismic Indicators of Fluids in Sediments.

Seismic surveys are today a fundamental tool when it comes to explore and interpret the subsurface. Fluids such as gas and oil are identified and mapped across the globe with the technology. The hydrocarbons in the subsurface can look very different, but share similar characteristics with its effect on the seismic data due to dramatic change in medium velocity where hydrocarbons are present.

1.2.3.1 Acoustic Masking / - Turbidity.

Acoustic masking is where an area of the seismic data with low reflectivity or with highly distortion or disturbed reflectors due to scattering of energy by gas (Fig. 5) (Andreassen et al., 2007; Judd & Hovland, 1992). Often reflections may feature a "***pull-down*** effect" in the border with an area with acoustic masking (Fig. 5).

When acoustic masking occur in a vertical or near-vertical fashion it is called a gas pipe or gas chimney and represent a zone of high vertical fluid flux (Fig. 5) (Andreassen et al., 2007). ***Gas pipes*** are sub-vertical, circular and narrow, usually less than ~200 m wide (Andreassen et al., 2007). Gas pipes are often close to bright spots or sub-circular depressions, which further signify their association as a fluid migration pathway (Fig. 5)(Løseth, Wensaas et al., 2011). ***Gas chimneys*** are a

similar feature to gas pipes, and is describes as vertical zones of fluid flux with low trace-to-trace coherency, low reflection amplitude and highly variable dip- and azimuth, where its sides correspond to the lateral termination of seismic blanking and up-bending strata (Andreassen et al., 2007; Ligtenberg, 2005; Ligtenberg et al., 2003; Plaza-Faverola, Bünz et al., 2011). Gas chimneys can appear in the seismic as as diffuse shadows, funnels, cigars and obelixes (Løseth et al., 2009).

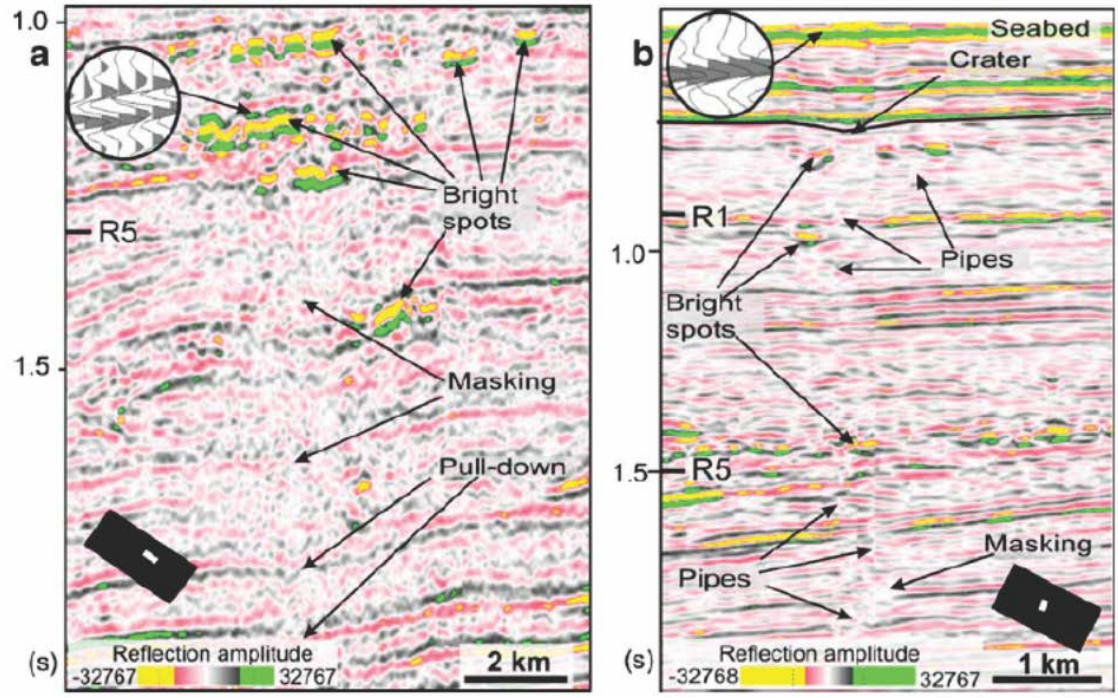

Fig. 5: Two seismic profiles showing different features of indications of hydrocarbons in a seismic profile. a) Seismic profile showing a pronounced zone of acoustic masking, associated bright spots and pull-down of underlying reflections. b) Seismic profile showing acoustic pipes interpreted to represent fracture pathways for gas-bearing fluids, and associated acoustic masking and bright spots. The small insets in the upper left corners of a and b show variable area/wiggle trace displays of a bright spot in a) and of the seafloor reflection in b). From Andreassen et al (2007).

1.2.3.2 Seismic Indicators Hydrocarbons in Seismic Data.

Hydrocarbon's velocity affect have two differences. It will create either a very powerful acoustic coefficient or a negligible one. Different varieties of this combination acknowledged in the scientific community is here explained.

In the seismic data relative powerful, compared to other reflectors in the seismic data, reflectors are called ***enhanced seismic reflector***. A ***bright spot*** is when there is a negative amplitude enhanced seismic reflector immediately followed by a positive enhanced seismic reflector (Fig. 5 & Fig. 6) (Andreassen et al., 2007).

A special case of bright spot is the ***flat spot***. In case of a bright spot is generated because of hydrocarbons there will be either a gas-water, or a gas-oil and then an oil-water border vertically under it. If the seismic resolution is good enough for the reflection to be visible this border will be, relative, flat due to buoyancy, i.e. in normal situations gas will be on top of oil, oil will be on top of water, due to density. This

acoustic reflector is therefore called a flat spot (Fig. 6) (Andreassen et al., 2007; Løseth et al., 2009).

The opposite of a bright spot is called ***dim spot***. A dim spot, or zone, is where there is a local acoustic masking for any reason, i.e. a local decrease in amplitude (Løseth et al., 2009)

Phase reversal is when a seismic reflector changes phase, or amplitude, from positive to negative along a continuous reflector, i.e. a seismic reflector goes from positive to negative value (Løseth et al., 2009).

Flat spots, bright spots, pull-down and phase changes are all because of their association with gas often called **D**irect **H**ydrocarbon **I**ndicators – DHI (Ligtenberg, 2005)

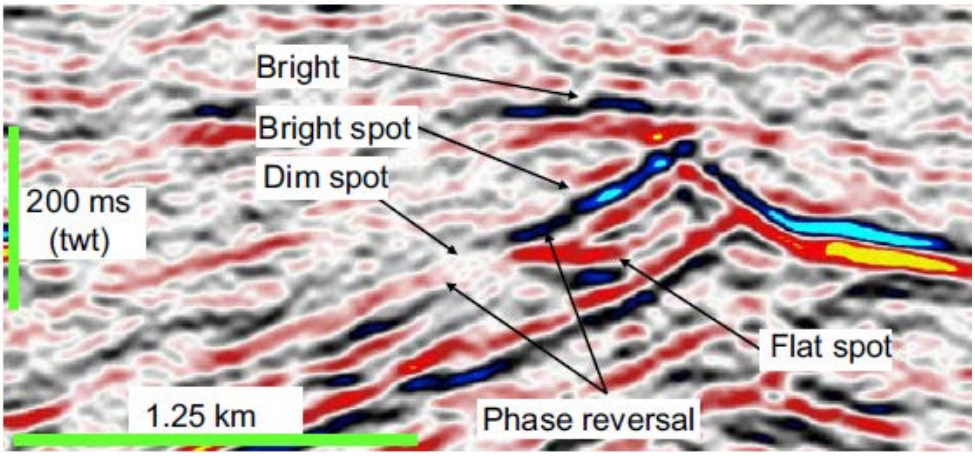

Fig. 6: Bright -, dim - and flat spot suggest the presence of hydrocarbon in a reservoir. From Løseth et al. 2009.

1.2.4 Focussed fluid release indicators on the seafloor.

"According to latest consensus, normal pockmarks are inferred to result from focused, continuous or sporadic gas and pore-water seepage, but exactly how they are formed is still a matter of debate" Hovland, Jensen et al. (2012).

Concave, spherical, crater-like depression made of subsurface fluids flowing out of the subsurface exists on the world ocean floor in many regions. The so-called-pockmarks vary in size from for example: 1-10m wide and less than 0.6m deep to 700m wide and 45m deep (Hovland, 2001).

Hovland concluded (2001) that pockmarks are an indication of a hydraulically active seabed. The fluid that is emitted can be of different types of gas, water or mud (Hovland, 2001). Further proof of active pockmarks at the seafloor are being made in connection to focused fluid flow in the sub seafloor documented in so-called gas pipes or gas chimneys. They occur quite frequently directly beneath a pockmark on the seafloor (Andreassen et al., 2007; Plaza-Faverola et al., 2011). They spread in abundance over some of the hydrocarbon fields, e.g. the Gullfaks field in the North Sea and in Nyegga close to the Ormen Lange deep-water gas field. Pockmarks can

be used as an indicator of hydrocarbon seepages (Hovland, 2001; Plaza-Faverola, Bünz et al., 2012).

There are also some species of deep-water corals and bacteria that do feed on gas seepage in pockmarks. For example, corals can be found in the immediate downstream area of pockmarks and the amount of bacteria increases in proximity to the pockmark (Hovland et al., 2012).

1.2.5 Fault Related Fluid Migration.

Faults and fault zones makes up an important potential fluid migration pathway in many of the world's basins (Ligtenberg, 2005; Løseth et al., 2009). It is important to note before continuing that fault can also act as an impermeable border separating a theoretical reservoir, therefore faults can be interpreted as either non-conductive or conductive (Ligtenberg, 2005). If there is migration through a fault, it can be through only a weakness zone or the whole fault plane (Ligtenberg, 2005; Løseth et al., 2009). In the seismic, the fault itself is often too narrow to be visualized on the seismic data; a vertical section of lateral discontinuous reflectors with vertical offset, to a "matching" reflector, are therefore interpreted as faults in the dataset (Løseth et al., 2009). If there are other DHIs in along the fault, it is used as an indication that the fault is acting as a fluid migration pathway (Løseth et al., 2009).

1.2.5.1 Polygonal faults

Polygonal fault system is a non-tectonic, non-gravitational generated normal faults with multi-directional and small throw (<80m), found within passive margin sedimentary basins around the world (Berndt, Bünz et al., 2003; Ostanin, Anka et al., 2012; Watterson et al., 2000). The formation mechanisms is still discussed between different mechanics, with the consensus that the faults are made from fluid expulsion. (Berndt et al., 2003; Ostanin et al., 2012; Watterson et al., 2000).

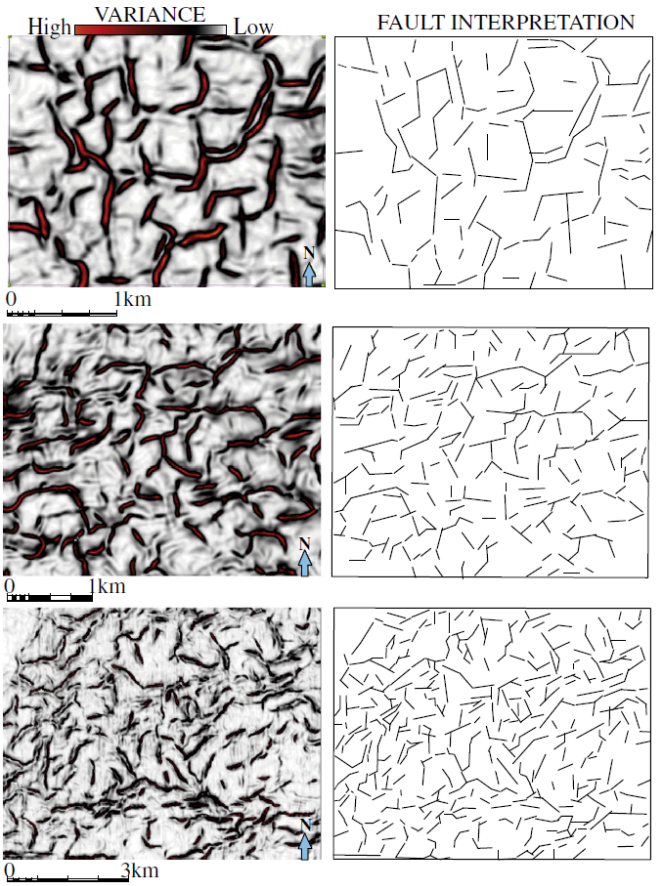

Fig. 7: Variance map and interpretation of iconic 'honeycomb' structures of interpret polygonal fault system. From Ostanin et al., (2012).

2 Geological Setting.

2.1 Introduction.

This master thesis uses the survey ST0825 that per NPD field organization lies in the 7019-2&3 and 7119/12 blocks of the SW Barents Sea, in a North-South direction. The study area lies 160 km north of Tromsø, in ~200 m water depth of the SW Barents Sea. The Barents Sea is with ~1,3 mill km^2 the world largest continental-shelf seas. It hosts some of the deepest sedimentary basins in the NW corner of the Eurasian plate (Basov et al., 2009; Doré, 1995; Faleide, Gudlaugsson et al., 1984). It borders the Atlantic Ocean in the west, the Norwegian Sea and Norway in the south west, the Kara Sea and Novaya Zemlya in the east, the Pechora Sea in the south east and the Arctic Ocean, Svalbard and Franz Joseph Land in the north. Geophysical investigations began on the Norwegian side of the Barents Sea in the 1960s and the Norwegian Petroleum Directorate (NPD) opened for drilling in 1980. The first hydrocarbon discovery was made in 1982 – Askeladden (Snøhvit field) (Doré, 1995; Gabrielsen, 1984; NPD, 2013). In the following, all ages for the stratigraphic sections refer to the International Stratigraphy Chart v2015/01, and for convenience there is a copy in the Appendix (Fig. 30).

2.1.1 Paleozoic.

Old tectonic activity during Devonian – Early Carboniferous sets the structural framework for the present basement of the Barents Sea (Basov et al., 2009; Gudlaugsson, Faleide et al., 1998; Henriksen, Bjornseth et al., 2011).

The Caledonian orogeny started in Middle Ordovician with the tectonic climax during Silurian (Basov et al., 2009; Henriksen, Bjørnseth et al., 2011). The Iapetus Ocean closed and paleo-continents Laurentia, Avalonia and Baltica bounded and created the Laurasian continent, Fig. 8 (Basov et al., 2009; Doré, 1995; Gabrielsen, Færseth et al., 1990; Henriksen, Bjørnseth, et al., 2011; McKerrow, Mac Niocaill et al., 2000). Since Caledonian orogeny a N-S structural trend with later basins and structural features existed, as exemplified by some rift basins and half grabens which developed off the Finnmark coast (Basov et al., 2009; Gabrielsen et al., 1990; Gudlaugsson et al., 1998; Henriksen, Bjornseth, et al., 2011)

In early Devonian, the depositional environment in the SW Barents Sea largely depends on the ongoing orogeny and the erosion of metamorphic structures. The orogeny led to deposition of clastic sediments in the intracratonic basins; at this time today's SW Barents Sea was predominantly land and located at sub-tropical 20-30^{o}N (Fig. 8 & Fig. 15) (Basov et al., 2009; Henriksen, Bjornseth, et al., 2011).

In early Carboniferous, the western Barents Sea region had very different depositional environments: Highlands, alluvial and fluvial plains, marshes and predominantly easterly prograding delta (Fig. 15) (Basov et al., 2009; Henriksen, Bjornseth, et al., 2011). These sedimentary systems were partly controlled by active horst-graben tectonics and basin formations (Basov et al., 2009; Henriksen, Bjornseth, et al., 2011). By late Carboniferous, the area experienced a regional subsidence, which led to a shallow-water and more normal shelf seas and basin conditions (Fig. 8 & Fig. 15) (Basov et al., 2009; Gabrielsen et al., 1990).

In early Permian, shallow basins in the SW Barents Sea show predominately evaporites and evaporite clasts (Basov et al., 2009; Doré, 1995). These evaporites came from the eastern Barents Sea, where evaporites were dominant. Evaporation was high under a warm and arid climate (Basov et al., 2009; Doré, 1995). However, during the Permian the sea level changed quite often and therefore the depositional environment. It was affected by glaciations and related sea level changes, which had an impact on shallow and deeper-water shelf depositional conditions (Fig. 8 & Fig. 15) (Basov et al., 2009; Henriksen, Bjornseth, et al., 2011).

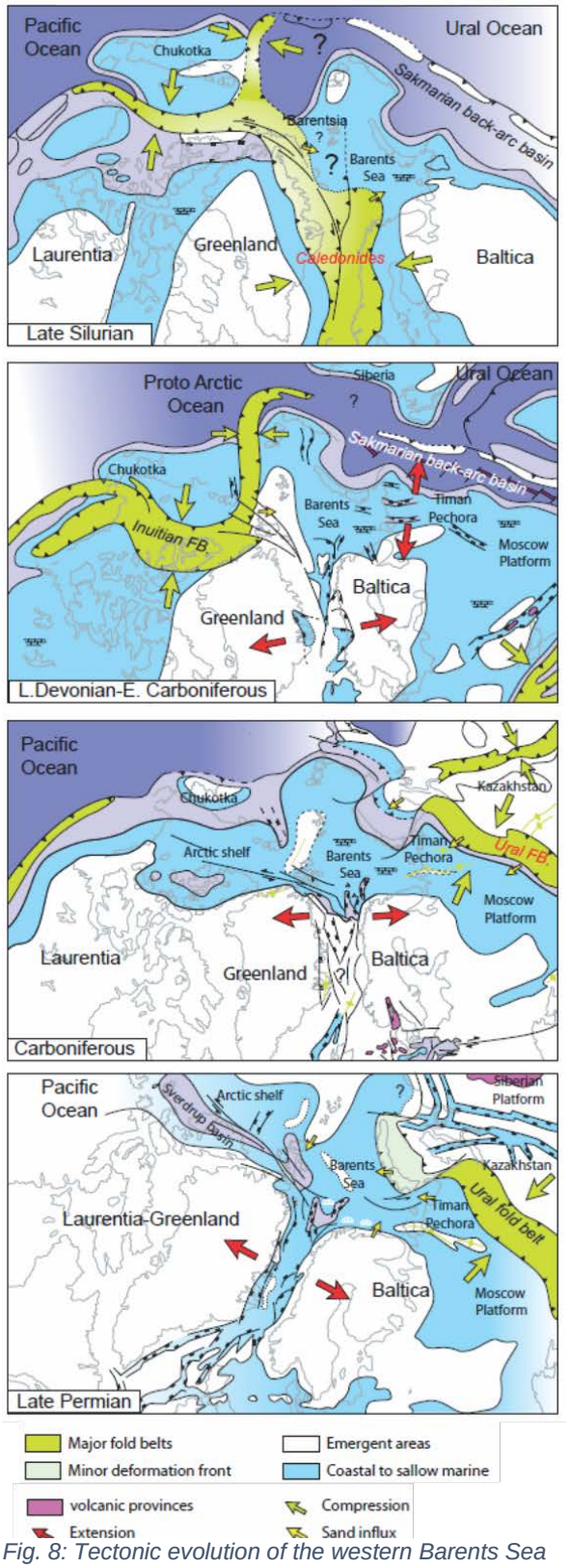

Fig. 8: Tectonic evolution of the western Barents Sea and surrounding area. Paleozoic time. From (Basov et al., 2009)

2.1.2 Mesozoic.

In the Triassic, there were little tectonic activities compared to the rest of Mesozoic; however, some minor tectonic events can be recognised alongside with regional subsidence (Fig. 9) (Basov et al., 2009; Gabrielsen et al., 1990; Henriksen, Bjornseth, et al., 2011). The Eurasian plate, at the time Pangea, continued to drift northwards; and by Late Triassic Mid Norway was around 45°N and by late Jurassic at ca. 54°N (Basov et al., 2009; Doré, 1995; Torsvik, Carlos et al., 2002). In early Triassic, the western Barents Sea shelf with its shallow water region was not

connected to the east Barents Sea but connected in the west with the early development of the Atlantic (Fig. 9) (Basov et al., 2009; Henriksen, Bjornseth, et al., 2011; Torsvik et al., 2002). Even though the area as a whole was a shelf there were locally deeper basins, i.e. Hammerfest Basin (Basov et al., 2009; Henriksen, Bjornseth, et al., 2011). In contrast to the early, middle to late – Triassic the southern Barents Sea experienced uplift; because of the continuing spreading between Greenland and the Eurasian plate, Fig. 9 (Basov et al., 2009). This uplift led to erosion and westward propagation of the Barents Sea and a coastal and near-shore depositional environment developed in the south western Barents Sea (Basov et al., 2009). The sandstones, with interbedded mudrocks, were deposited along the NE-SW trending coastline on a shelf environment (Fig. 15) (Basov et al., 2009).

The Jurassic started with periodically flooded plains and shallow-marine depositional environments in the west basins, especially southern Hammerfest Basin was a major depocentre (Fig. 15) (Basov et al., 2009; Henriksen, Bjornseth, et al., 2011). The sea-level rise during early Jurassic and in the middle Jurassic flooded plains, but uplift made the central Barents Sea once again to rise above sea-level (Fig. 9) (Basov et al., 2009; Henriksen, Bjornseth, et al., 2011). Even though there was uplift there are also deposits which suggest that a marine connection between the eastern and western marine basins existed (Basov et al., 2009). When the transgression reached its maximum stage in late Jurassic, the Barents region showed a shelf like marine environment with predominantly clayey sediments, Fig. 9 (Basov et al., 2009).

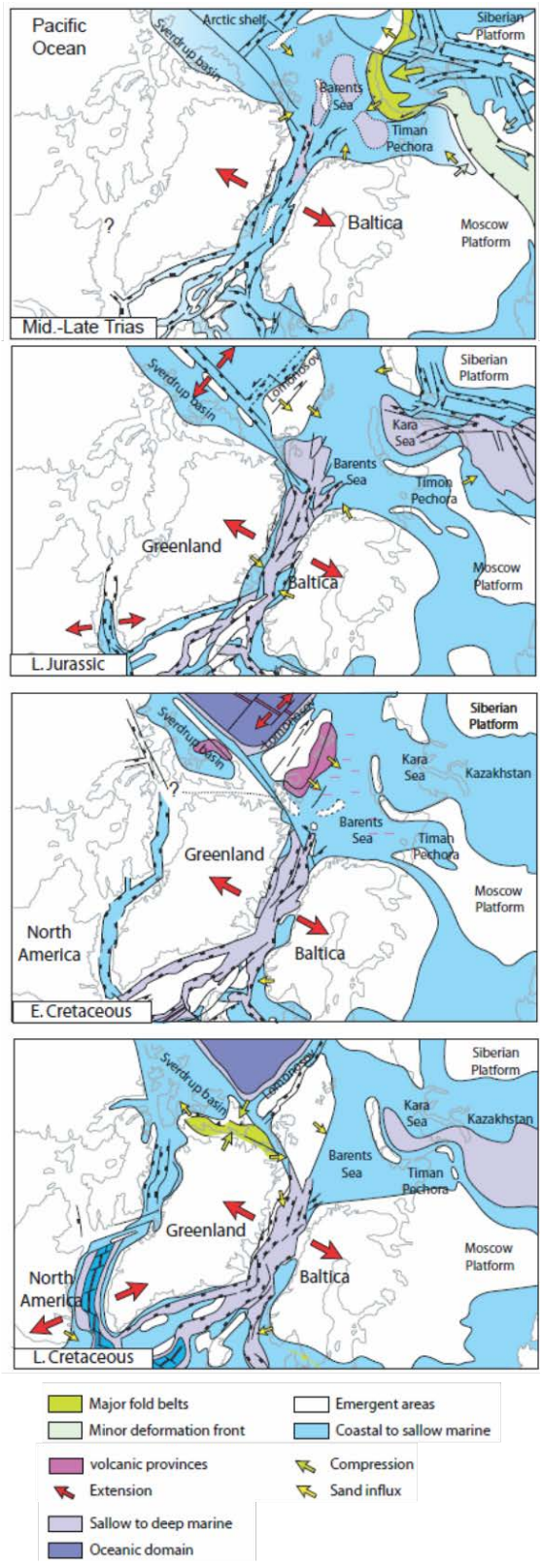

Fig. 9 Tectonic evolution of the western Barents Sea and surrounding area. Mesozoic time. From (Basov, Ebbing et al., 2009)

In Cretaceous the regression continued. However, tectonic activity and the creation of the Arctic Ocean also caused uplift and tilting north of the Kara Sea, which caused terrigenous supply to the western and deeper parts of the Barents Sea, Fig. 15 (Basov et al., 2009). In early Cretaceous, there was a cooler climate with repeated glaciations. The uplift in the north during the middle Cretaceous; created large deltas towards the subsiding basins in the south, e.g. Tromsø - and Harstad Basin. In combination with the

tectonic activity, some magmatic activity existed in the Cretaceous period, documented by sill intrusions in the southern Barents Sea (Basov et al., 2009; Henriksen, Bjornseth, et al., 2011). Rifting episodes in Cretaceous led to rapid subsidence in the western Barents Sea; further developing some of the major basins in the area e.g. Harstad and Tromsø Basin (Basov et al., 2009; Henriksen, Bjornseth, et al., 2011). The Eurasian plate drifted further north and Tromsø is now located at just below 60°N and by this time the structural elements in the SW Barents Sea all were established (Basov et al., 2009; Henriksen, Bjornseth, et al., 2011; Torsvik et al., 2002) .

2.1.3 Cenozoic.

The spreading of Norwegian-Greenland Seas continued to move northward in Palaeogene while the basins in western Barents Sea continued to subside (Fig. 10) (Basov et al., 2009) The break-up and creation of the North Atlantic margins started in Paleocene-Eocene (Basov et al., 2009; Henriksen, Bjornseth, et al., 2011; Martinsen & Nøttvedt, 2008; Torsvik et al., 2002). Currently the Eurasian and American plate have a half-spreading velocity of ~1cm/yr. (Basov et al., 2009; Torsvik et al., 2002). From Late Cretaceous (Campanian) to Paleocene Tromsø drifted from around 60° to 69°N, which is it's approx. current position (Martinsen et al., 2008; Torsvik et al., 2002). Later, in Neogene, some uplift took place caused by large-scale plate movements. However, the uplifted areas were heavily eroded and consequently there is little sediments left from this period in the region (Basov et al., 2009; Henriksen, Bjornseth, et al., 2011; Martinsen et al., 2008). Nevertheless, the basins in the SW Barents Sea continued to subside and sediments were deposited here, e.g. Harstad, Tromsø and Sørvestsnaget Basin Fig. 15 (Basov et al., 2009; Martinsen et al., 2008).

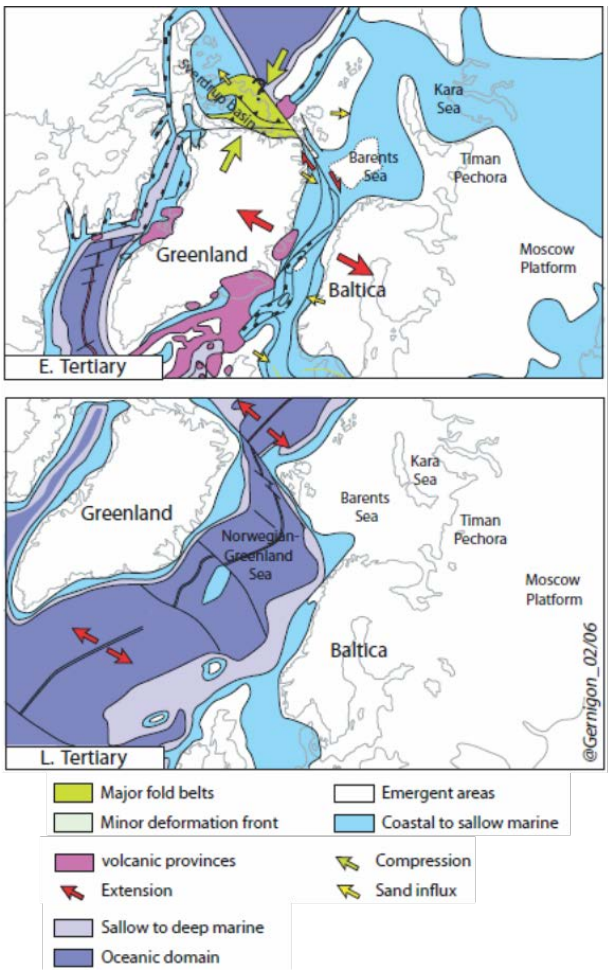

Fig. 10: Tectonic evolution of the western Barents Sea and surrounding area. Cenozoic time. Tertiary is the time from 66 Ma to 2.58 Ma, an elder term for Cenozoic. From (Basov et al., 2009)

The Barents Sea experienced several glaciation cycles during the late Cenozoic – late Pliocene (Basov et al., 2009; Martinsen et al., 2008). From the late Pliocene to Pleistocene there have been three stages of glaciations with varying maximum extent and ice sheet thickness, the last stage started 1 Ma consisted of at least five shelf-edge glaciations (Basov et al., 2009). The youngest major glaciation, the late Weichselian glaciation, covered the whole Barents Shelf and its maximum extent was

reached at ~22 ka. The deglaciation started at ~19 ka (Winsborrow, Andreassen et al., 2010). Because of these glaciations, which are accompanied by major erosional events of the ice sheet on the shelf, the sediment cover in the Barents Sea and thus the study area consists only of a thin layer of Quaternary sediments (<100 -300m) (Winsborrow et al., 2010). The whole Barents Sea region has clear glacial erosional indications, e.g. iceberg ploughmarks, mega-scale glacial lineations, grounding wedge zones and much more (Andreassen, Winsborrow et al., 2014; Bjarnadóttir, Winsborrow et al., 2014; Winsborrow et al., 2010). Because these glaciations eroded much of the regional sediment cover an erosional boundary exists between the top glacial sediments and directly beneath underlying rocks (Mesozoic-Tertiary), also known as the upper regional unconformity (URU) (Basov et al., 2009; Henriksen, Bjornseth, et al., 2011; Martinsen et al., 2008)

2.2 Structural Elements.

The structural geology in the study area shows some dominant elements such as the Finnmark Platform, Troms-Hammerfest fault complex, Hammerfest Basin and Ringvassøy-Loppa fault complex, from north to south respectively (Gabrielsen et al., 1990)

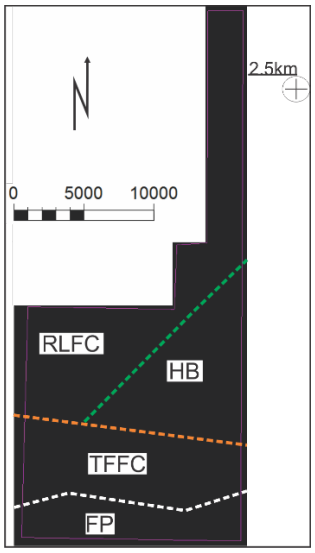

Fig. 11: Projected position of borders between structural elements in the survey. FP = Finnmark Platform. TFFC = Tromsø Finnmark Fault Complex. HB = Hammerfest Basin. RLFC = Ringvassøy Loppa Fault Complex. The circle with the cross indicate the projected position of the well 7119/12-1. The location of the survey is indicated in Fig. 12.

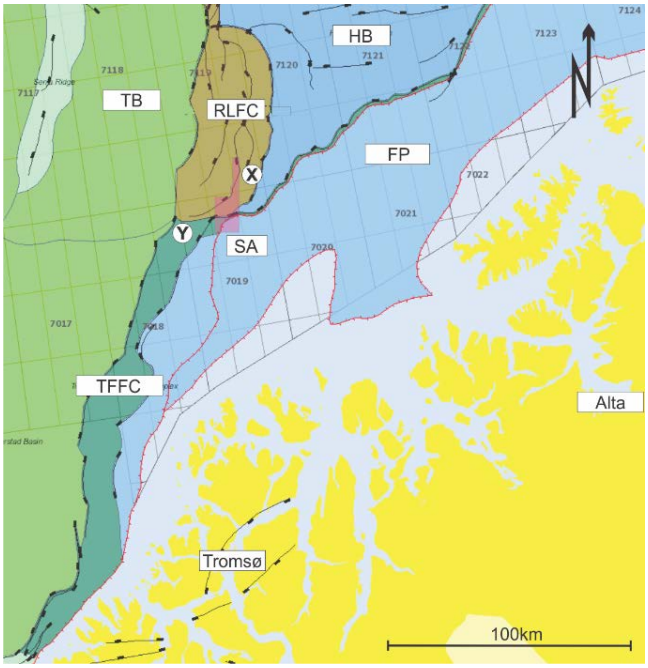

Fig. 12: Location of study area and structural elements. TFFC = Tromsø-Finnmark Fault Complex. SA = Study Area. FP = Finnmark Platform. RLFC = Ringvassøy-Loppa Fault Complex- TB = Tromsø Basin. HB= Hammerfest Basin. The red area indicate the survey. Note that the structures are not limited to the area covered in the picture. X indicate position of well 7119/12-1 & Y indicate position of well 7019/1-1. Modified from http://gis.npd.no/.

2.2.1 Finnmark Platform (FP).

Finnmark platform has been established already in the Late Paleozoic – Permian, (Gabrielsen et al., 1990). The platform was heavily eroded; thus the Quaternary sediments in the western part rest directly on Jurassic and Triassic formations (Fig. 13) (Gabrielsen et al., 1990). The base of the platform is assumed to be from Precambrian or the Paleozoic and was affected by the Caledonian orogeny (Gabrielsen et al., 1990).

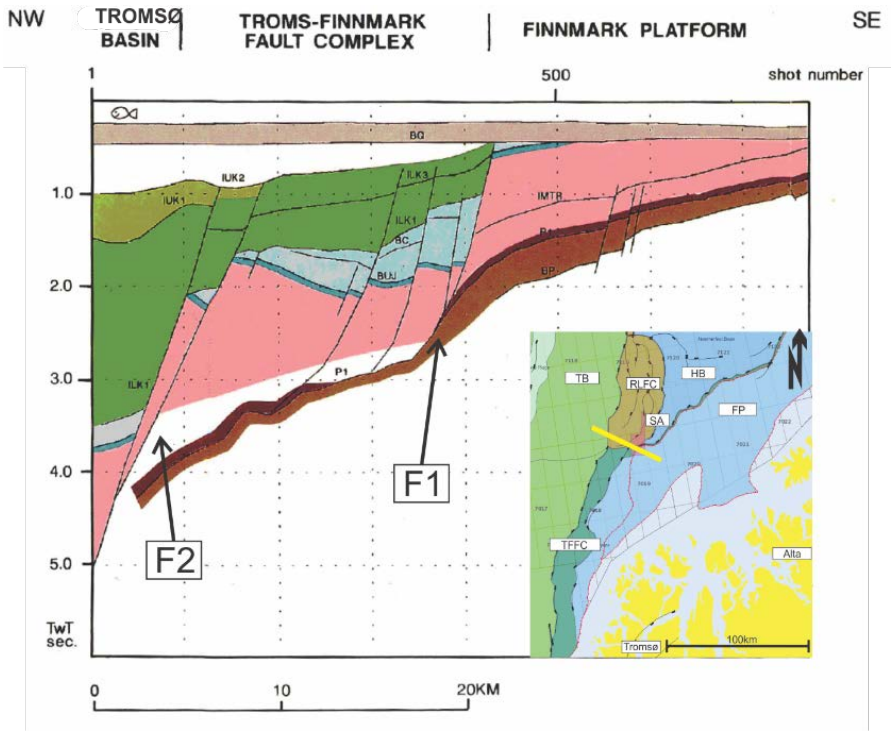

Fig. 13: Profile shot through Tromsø Basin - TFFC - Finnmark Platform, going through the study area. BP = Near Base of Permian, brown coloured. P1 = Near Top Permian. IMTR = Intra Middle Triassic, pink coloured. BUJ = Base of Upper Jurassic, coloured blue – light blue. ILK1 & 3 = Intra Lower Cretaceous (Hauterivian?) - Intra Lower Cretaceous, coloured green. IUK1 & 2 = Intra Upper Cretaceous Cenomanian(?)-Campanian (?) coloured yellow-green. BQ = Base quaterny, coloured gray. The boundary between Jurassic and the Triassic is not interpreted. Modified from Gabrielsen et al., 1990. F1&2 stands for fault 1 & fault 2.

2.2.2 Tromsø-Finnmark Fault Complex (TFFC).

The TFFC runs roughly parallel to the coastline of Troms and Finnmark counties (Fig. 12) and makes up the border between: Harstad Basin and Finnmark Platform; Ringvassøy-Loppa High Fault Complex and Finnmark Platform; and Hammerfest Basin and Finnmark Platform. TFFC is the structure, which borders the coast and the basins in the SW Barents Sea. As such it has been active in different periods: pre-Permian, Late Jurassic, Early Cretaceous, Late Cretaceous, and has been reactivated several times until Eocene (Gabrielsen et al., 1990).

2.2.3 Hammerfest Basin (HB).

Named after Hammerfest town, Hammerfest Basin (HB) is with 6-7 km thickness below seafloor a relative shallow basin which can be traced back to Late Devonian – Early Cretaceous tectonic activity (Gabrielsen et al., 1990). It has both deep high-angle faults along the margins and listric normal faults detached above Permian –

more centrally in the basin; informally named Hammerfest Basin fault complex (Gabrielsen et al., 1990).

2.2.4 Ringvassøy-Loppa Fault Complex (RLFC).

Named after Ringvassøy and Loppa islands the Ringvassøy-Loppa Fault Complex is the border between Tromsø Basin, Hammerfest Basin, Loppa High and Finnmark platform. It is also the border to the TFFC. It's development has been dated to mid Jurassic, but it may have been active before, and have been reactivated in Late Cretaceous and Cenozoic (Gabrielsen et al., 1990). The southern section is dominated by normal faults showing a north-south trend (Gabrielsen et al., 1990).

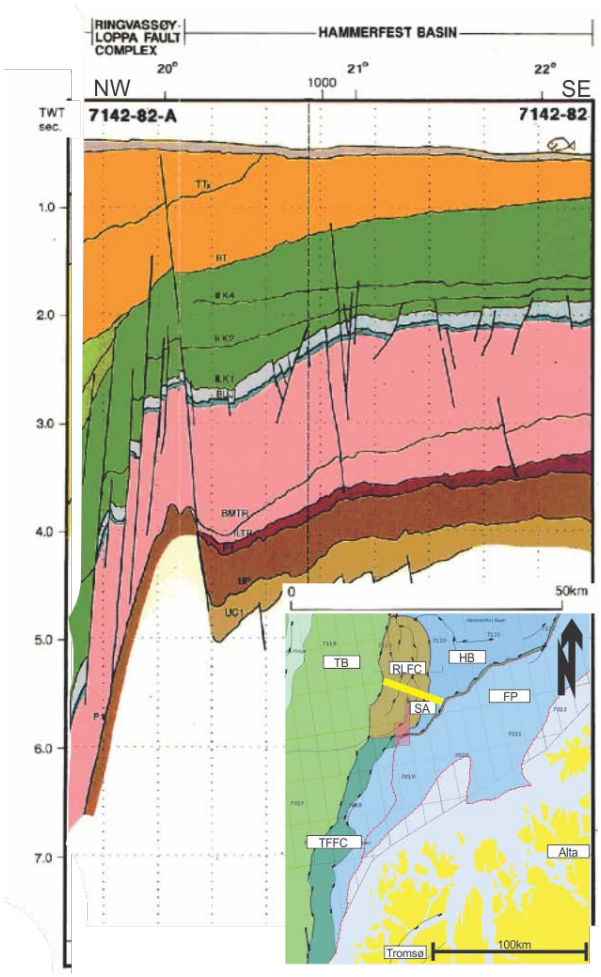

Fig. 14: Profile of RLFC – HB, from seismic lines 7142-82-A & 7142-82. UC1 =? Late Carboniferous, coloured olive. BP = Near Base of Permian, coloured brown. P1 = Near Top Permian, coloured dark red. ILTR = Intra Lower Triassic & BMTR = Base of Middle Triassic, both coloured pink. BUJ = Base of Upper Jurassic, coloured blue & light blue. ILK1-4 = Intra Lower Cretaceous, coloured green. IUK 1-2 = Intra Upper Cretaceous, coloured light green. BT = Base of Tertiary & TTx = Top of Paleocene, coloured orange. BQ = Base Quarternary coloured grey. Modified from Gabrielsen et al., 1990.

2.3 Lithostratigraphy.

The study area lies in four different structural elements, which are FP, TFFC, HB and RLFC. One well 7119/12-1 is located approximately 2.5 km away from this thesis' survey, will be used in an attempt to describe the lithostratigraphy as good as possible (Fig. 11) . The resulting lithostratigraphy is using the official NPD nomenclature defining lithostratigraphical units (see NPD 1988). The control lithostratigraphy is taken from Norwegian Offshore Stratigraphic Lexicon – South Western Barents Sea – SW, since the study area lies just southwest of Loppa High (NORLEX). The oldest lithology group the well 7119/12-1 penetrate is the Kapp Toscana Group at 2658 mbsl, which belongs to Bethonian – Middle Jurassic. This log make it also possible to describe the petrophysical and geophysical characteristics of the different groups and changes within.

2.3.1 Definition of lithostratigraphy.

Stratigraphy is the study of layers of sedimentary soil or rock, i.e. the study of strata. Lithostratigraphy is the part in stratigraphy, which study strata based on its lithology, and make up units with similar lithological characteristics, i.e. physical and chemical properties. Nichols (2009) describe lithostratigraphy units as follows:

"..a body of rock can be distinguished and defined by its lithological characteristics and its stratigraphic position relative to other bodies of rock: these are lithostratigraphic units.. The units can be classified into a hierarchical system of members, formations and groups that provide a basis for categorising and describing rocks in lithostratigraphic terms." Nichols, p. 302. 2009.

To clarify this hierarchy: Group is the highest, then formation and lowest is the member. I.e. in general, one group consist of one or more formations and a formation is made up of one or more members.

2.3.2 Billefjorden Group.

The Billefjorden Group contains the Soldogg -, Tettegras - & Blærerot formation, the presence of the group is from Viséan to Serphukhovian, which is of Early Carboniferous age, (Fig. 15) (Larssen, Elvebakk et al., 2002).

According to Larssen et al. (2002) from base of formation and upwards, the Soldogg Formation contains coal medium- to course grained sandstone, sometimes conglomeratic and minor siltstones. Soldogg – is followed by Tettegras Formation, which consist of stacked metre-scale fining-upwards cycles of sandstone, siltstone, claystone and coal. Lastly the Blærefot Formation consist of fossiliferous limestones, marine shales and fine- to medium-grained fluvial and marine sandstones, respectively (Larssen et al., 2002).

These deposits suggest that from Viséan to Serphukhovian the depositional environment in the west Finmark Platform can be characterised as a transition from

continental fluvially dominated to transitional continental to marginal marine deposits (Fig. 15) (Larssen et al., 2002).

2.3.3 Gipsdalen Group.

The Gipsdalen Group contain the Ugle -, Falk- & Ørn Formation, however in our area it is only the Ørn Formation, which is present; from Moscovian to Sakmarian. It represents Late Carboniferous to Early Permian time (see also 'Moscovian' in Fig. 15) (Larssen et al., 2002).

The Ørn Formation contains shallow marine carbonates on the platform but interbedded carbonates and evaporites on the distal ramp to basinal settings, which suggests the existence of a transitional region between the two depositional environments (Larssen et al., 2002).

These deposits indicate that the Ørn formation developed in a shallow to deeper marine depositional environment. (Fig. 15, Viséan to Asselian, a time when the region shows a highly variable water depth).

2.3.4 Bjarmeland Group.

The Bjarmeland Group contains the Polarrev -, Ulv - & Isbjørn Formations, however in our area it is only the Isbjørn Formation which is present, in Artinskian, which represents early Permian (NORLEX).

The Isbjørn Formation contain limestones, grainstones, packstones and some thin intervals of silty wackestone (Dalland, Worsley et al., 1988).

This indicate a depositional environment of an inner shelf, cool-water carbonate platform (see Asselian Fig. 15) (Dalland et al., 1988).

2.3.5 Tempelfjorden Group.

The Tempelfjorden Group contains the Røye - & Ørret Formations and both should be present in the study area, Kungurian to Wuchiapingian, which represents late Permian (NORLEX).

The Røye Formation contains fine-grained highly silicified mudstones and limestones. The formation is followed by the Ørret Formation, which contains siliciclastic sediments such as shale, siltstone and sandstone (Dalland et al., 1988).

This indicate a depositional environment of cool-water, temperate shelf and basinal environments (see Wordian Fig. 15) (Dalland et al., 1988)

2.3.6 Ingøydjupet Group.

The Ingøydjupet Group contains the Havert -, Klappmyss -, Kobbe - & Snadd Formations, and is present at Induan to early Norian, which is of Triassic age (Dalland et al., 1988). Havert - and Kobbe Formation should both be in the study area (NORLEX).

This group contains shale, claystones, siltstone, sandstone, carbonate and coal, with the dominant being the shale and claystone. The Havert Formation contains shales with interbedded siltstones and sandstones with two coarsening upwards sequences (Dalland et al., 1988). The Kobbe Formation consist of shale, siltstone and carbonate cemented sandstone, respectively (Dalland et al., 1988).

The deposits indicate a coastline depositional environment for the lower part of the group going to deltaic conditions. (see Induan – Triassic in Fig. 15) (Dalland et al., 1988).

2.3.7 Kapp Toscana Group.

The Kapp Toscana Group contains Furuholmen -, Tubåen -, Nordmela - & Stø Formation, and all of them should be present in the study area (NORLEX). This group consist of formations from early Norian to Bajocian, which is Upper Triassic to Middle Jurrasic (Dalland et al., 1988).

The group consists of sandstones, shale and coal, whereas the group is dominated by the sandstone (Dalland et al., 1988). Fruholmen makes up the base and contains shales which gradually go into interbedded sandstones, shales and coals (Dalland et al., 1988). Tubåen Formation, following the group trend, is dominated by sandstones with some shales and a little coal (Dalland et al., 1988). Nordmela Formation has interbedded claystones, siltstone, shale and sandstones (Dalland et al., 1988). The Stø Formation is dominated by sandstones with thin units of shale and siltstone.

These deposits indicate a depositional environment of prograding deltaic systems in the late Triassic and later in early Jurassic a change towards a coastal marine environment (see Carnian to Bajocian in Fig. 15) (Dalland et al., 1988).

2.3.8 Adventdalen Group.

The Adventdalen Group consists of the Fuglen-, Hekkingen-, Knurr -, Kolje - & Kolmule Formations, and they should all be present in the study area (Dalland et al., 1988; NORLEX). The group consists of formations from late Callovian to Albian (Dalland et al., 1988; NORLEX). The group consists of shales, claystones, siltstone, dolomitic limestone and sandstones; the shale and claystone being the dominant in the group (Dalland et al., 1988). These deposits indicate a depositional environment of deep and quiet marine environment (Bajocian to Cretaceous in Fig. 15.) (Dalland et al., 1988).

2.3.9 Nygrunnen Group

The Nygrunnen Group consist of the Kviting - & Kveite Formations, and both should be present in the study area, but in the wellbores only Kveite is identified and were deposited from late Cenomanian to Maastrichtian – Upper Cretaceous (NPD, 2016a, 2016b, 2016c, 2016d, 2016e) (Dalland et al., 1988; NORLEX). The group contain claystone, limestone, and calcareous or sandy condensed sequences, in the study area it should be mostly claystones with thin limestone intervals (Dalland et al., 1988)

These deposits indicate a depositional environment of deep-shelf open marine (Albian – Upper Cretaceous Fig. 15.)(Basov et al., 2009)

2.3.10 Sotbakken Group.

The Sotbakken Group consists only of the Torsk Formation, which is present in the study. It was deposited from late Paleocene to middle Eocene – Paleogene (Fig. 15) (Dalland et al., 1988; NORLEX; NPD, 2016b). The group contains of claystone, siltstone and thin tuffaceous and carbonate layers, which should be present in the study area (Dalland et al., 1988).

These deposits indicate a deep shelf marine depositional environment, even though most of the Barents Shelf was at this time uplifted. (Basov et al., 2009)

2.3.11 Nordland Group.

The Nordland Group consist of the Kai-, Molo-, Naust- & Utsira formation, however the formations have not been identified in the well 7119/12-1. (Dalland et al., 1988; NORLEX; NPD, 2016a, 2016b, 2016c, 2016d, 2016e). The group consist of claystone and sandstone with appearances of pebble to boulder size metamorphic rocks (Dalland et al., 1988). The group was deposited during late Neogene to late Quaternary (Dalland et al., 1988; NORLEX). These deposits indicate an depositional environment on the slope of the continental margin and glacial marine influences (Dalland et al., 1988). In the Barents Sea the lower boundary of the Nordland Group is the Upper Regional Unconformity (URU) (Ostanin et al., 2012).

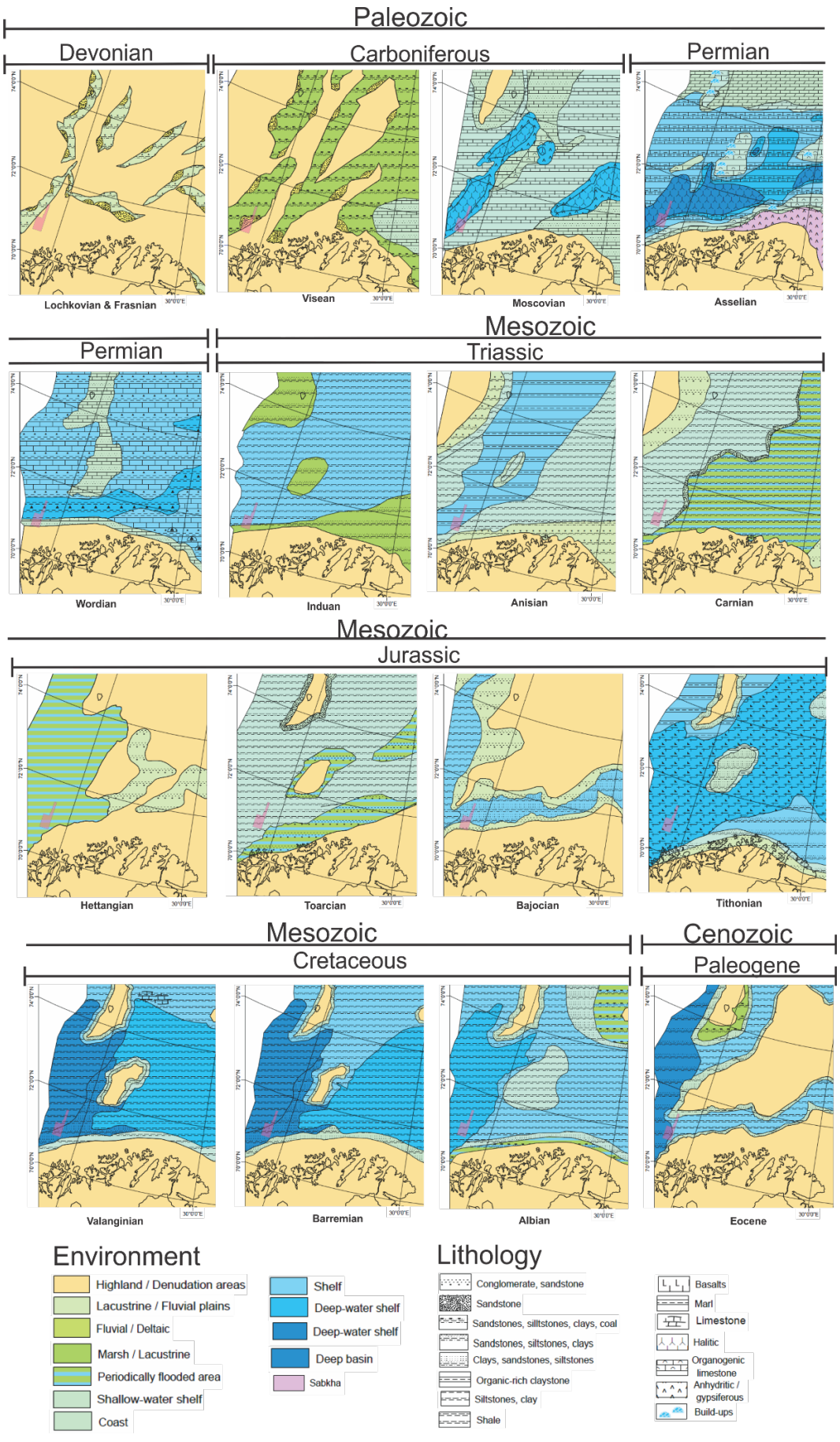

Fig. 15: Depositional environments. The Red area indicate the seismic survey. Modified from Basov et al., 2009.

3 Data & Methods.

3.1 Seismic and Well Data.

The data used in 4 Results & Interpretation comes from the seismic survey STP0825 and the well log from 7119/12-1, (NPD, 2016b, 2016f). The data presented here are from the header file of the survey, and it being a commercial survey the header is completed poorly.

The survey was completed by in 31.12.2008, with StatoilHydro ASA being the company responsible. The only technical information found is that the streamers are separated by 12.5m, i.e. dominant frequency, source frequency, shot spacing and etc are unknown. It is a total of 1000 inlines and 2385 crosslines and it is a 3D survey type.

The well 7119/12-1 was drilled as a wildcat exploration well, was completed in 10.10.1980 and was drilled by “Den Norske Stats Oljeselskap AS”-Statoil. The oldest penetrated formation is the Stø Formation – Early Jurassic at 3087 m TVD, more on this in 4.1 Seismic-stratigraphy.

3.2 Seismic Attribute Maps.

Different types of seismic attribute maps are used to enhance features and further improve the interpretation, the different types are here shortly introduced.

3.2.1 Structural Smoothing.

Structural smoothing were used to guide the horizon picking, as the area is heavily faulted. Petrel smoothes the input data to increase the continuity of the seismic reflectors along the structure, Petrel use the surrounding trace’s dip and azimuth to determine where a reflector continue or stop. (Schlumberger, 2014)

3.2.2 Variance (Edge Method).

This determine the amount of variance in the seismic. Discontinuities in the horizontal continuity of amplitude – edge, will be mapped and given a value 0-1 determined by how the trace differ from the others in its proximity. (Schlumberger, 2014)

3.2.3 RMS Amplitude.

The **R**oot-**M**ean-**S**quare –amplitude map is used to visualize, in a set volume, the location of higher amplitudes – bright spots. The computer square the amplitude of all the samples, then add them together and this sum is then square rooted. (Schlumberger, 2014)

3.3 Well Log Measurements.

A well log can show several different measurements, here a short introduction to the ones shown in this thesis.

3.3.1 Gamma Ray.

The gamma ray measures the natural radioactivity in the rocks –Geiger Counter. However, the industry standard is to use **A**merican **P**etroleum **I**nstitute –API as a measurement, the measurement is mostly used to determine the lithology, with other measurements, since different lithology have a varying amount of radioactivity (Rider, 2011). It's also often used to correlate wells and due to shale's high API the gamma ray log is also known as a shaliness scale, (Rider, 2011).

3.3.2 Density.

The bulk density log is used to estimate porosity, acoustic impedance, lithology, and more (Rider, 2011). The standard is to have the log values around 1.7 – 2.9 g/cm^3.

3.3.3 Acoustic/Sonic log.

The well log also measure the velocity laterally of the well. The acoustic log is per industry standard measured in microseconds per foot - (µs / ft.) and is used to: determine porosity, seismic calibration, acoustic impedance, lithology, source rock evaluation and more (Rider, 2011). In this master thesis, it is used to determine the depths of the different lithologies, see Heading 3.4.

3.4 Seismic Position Calculations of Lithostratigraphic Groups & Formations.

To determine the seismic position of the different groups and formations in the seismic survey, the velocity log from well 7119/12-1 was used. This log gather data, amongst them the P-wave's velocity and depth. The velocity data was then used to calculate the time position, in TWT ms, of the different groups and formations.

The velocity were gathered from the velocity log with its measured depth. The depth of the groups and formations were gathered from NPD's factpage – factpages.npd.no (NPD, 2016b). The velocity were then sorted, from top and down, to its group or formation. Then the average velocity to each group/formation were calculated, and converted with Equation 6 to meter per second (m/s). Then the velocity and depth were used to calculate the depth in microsecond **T**wo-**W**ay-**T**ravel (TWT), i.e. vertical position in the seismic.

Equation 6: $$\frac{time\ (\mu s)}{velocity\ (ft.)} = \frac{10^{-6}(s)}{0.3048\ (m)} \rightarrow \frac{0.3048}{x\ 10^{-6}}\ m/s$$

Equation 6: Conversion from of velocity speed from microsecond per feet (µs / ft.) to meter per second (m/s). x = the initial measurement in µs / ft..

Equation 7: $$\frac{depth\ (m)}{velocity\ (m/s)} = time\ (s) \rightarrow\ time\ x\ 2\ (s) = time\ (s\ TWT)$$

Equation 7: Calculation of ms TWT , from depth (m) and velocity (m/s).

Note the calculation provides the approximate TWT at the point of interest. One assumes that the point of the lithology is the closest most prominent amplitude reflection. The largest uncertainty is due to the fact that the well log is not exactly on the seismic line but ~2.5 km to the east and the velocity is averaged, Fig. 11: Projected position of borders between structural elements in the survey. FP = Finnmark Platform. TFFC = Tromsø Finnmark Fault Complex. HB = Hammerfest Basin. RLFC = Ringvassøy Loppa Fault Complex. The circle with the cross indicate the projected position of the well 7119/12-1. The location of the survey is indicated in Fig. 12. The velocity log were also deemed incorrect the top ~100m since the velocity were measured at 5700m/s and more. This work is shown in 4.1 Seismic-stratigraphy.

3.5 Artefacts.

In seismic 3D-datasets there will be to some degree systematic noise, which correlate with the acquisition geometry, i.e. the position of the receivers. This type of noise is called acquisition footprints, or simply footprints and is visualized as linear lines in the seismic (A-Fig. 16)(Bulat, 2005; Marfurt, Scheet et al., 1998) In a marine seismic 3D-survey the receivers are affected by ocean currents which slightly displace the receivers, making uniform sampling extremely difficult to achieve (Bulat, 2005). It is important that the interpreter are aware of footprints, since they can be misinterpreted to be gas pipes (Fig. 16).

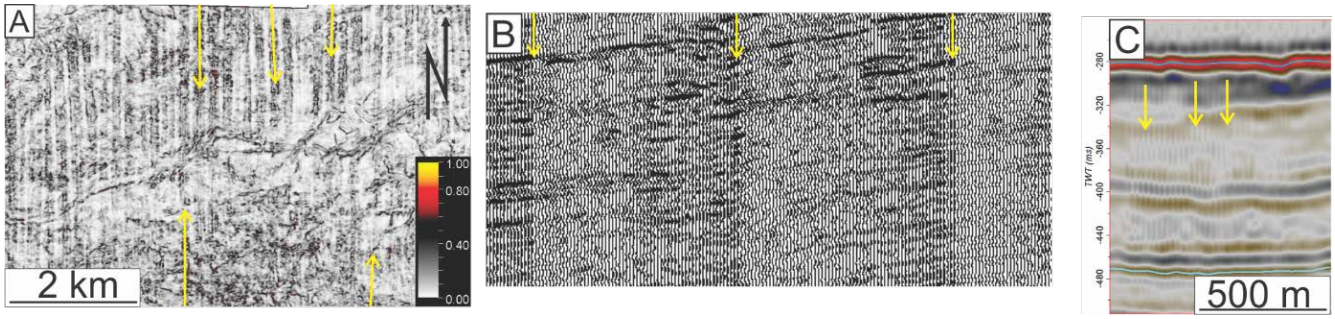

Fig. 16: Artefacts in the survey. A: example from a variance map. B: Example from a seismic line, shown with traces. C: How 'footprints' can visualize in the seismic. The yellow arrows in the pictures indicate survey footprints.

4 Results & Interpretations.

Observations from the dataset ST0825 are presented in this chapter, with focus on the seismic-stratigraphy, faults, amplitude anomalies and fluid flow features.

4.1 Seismic-stratigraphy.

Due to a complex tectonic history of the study area, the survey ST0825 is very varied, in terms of reflection strength and frequency. In this section the different lithological units' seismic will be described.

4.1.1 Position of Lithostratigraphies in the Seismic.

Table 1 shows the different lithostratigraphic units present in the well 7119/12-1, their thickness (m) and their estimated location in the seismic line 6964 ms TWT (Fig. 12-Orange line).

From the log of wellbore 7119/12-1 and the factpage of wellbore 7119/12-1 & 7019/9-1 Table 1 could be made (NPD, 2016a, 2016b). This data was then used to interpret the seismic line 6964 to map the different lithostratigraphic units, i.e. groups and formations (Fig. 17 –orange position). However, only the following lithostratigraphy were mapped: Nordland Group, Sotbakken Group, Nygrunnen Group, Kveite Formation, Adventdalen Group, Kolmule Formation, Knurr Formation, Hekkingen Formation, Kapp Toscana Group, Stø Formation and Nordmela Formation.

Seismic ms, used. (TWT)	Calculated ms (TWT)	Start, m	Name, group/formation	Avg. speed, m/s	Thickness, m
230	270	200	Seafloor	1500	25
275	300	225	Nordland GP	1500	240
450	500	465	Sotbakken GP Torsk FM	2458	345
750	832	810	Nygrunnen GP Kveite FM	2073	248
1025	1050	1058	Adventdalen GP Kolmule FM	2275	946
X	1736	2004	Kolje FM	2775	437
1925	2002	2441	Knurr FM	3243	57
2025	2030	2498	Hekkingen FM Krill Mbr	3387	76
2180	2080	2574	Alge Mbr	3175	36
2340	2103	2610	Fuglen FM	3018	48
2650	2129	2658	Kapp Toscana GP Stø FM	3586	min. 342
X	2375	3000	END wellbore.	X	X
2700	X	X	Nordmela FM	X	X

Table 1: Lithostratigraphy of the well 7119/12-1. Speed data average calculated from well log from wellbore 7119/12-1. Nordmela FM presence from well log 7119/1-1. The "Seismic ms used" is from the orange line in Fig. 17. It is used 1500m/s for the Seafloor and Nordland Group, because it is assumed to have a high seawater content - the measured average speed in the well log were 5700 m/s and higher which is assumed to be wrong.

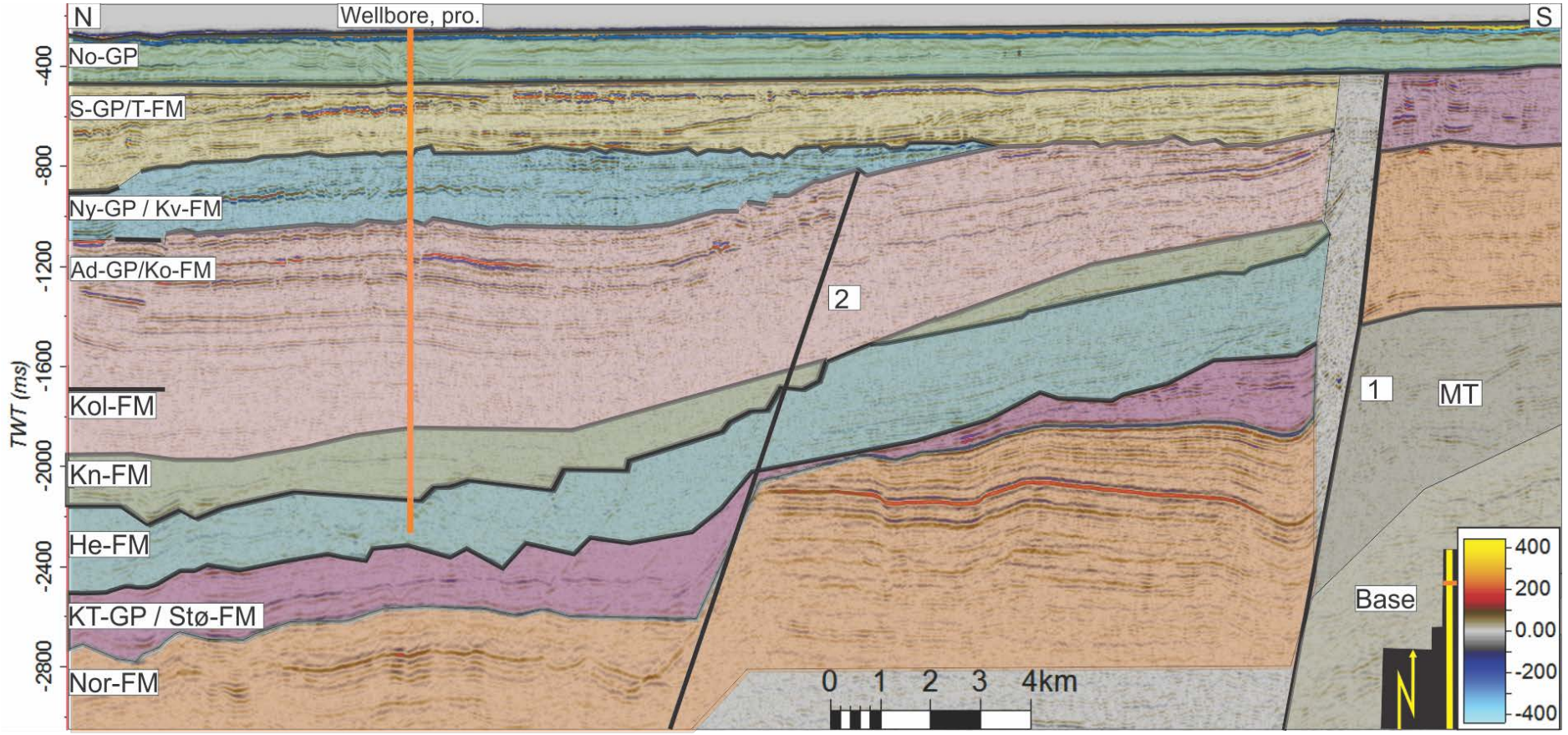

Fig. 17: The different lithological units marked in the seismic. GP = Group, FM = Formation, No = Nordland, S = Sotbakken, T = Torsk, Ny = Nygrunnen, Kv = Kveite, Ad = Adventdalen, Ko = Kolmule, Kol = Kolje, Kn = Knurr, He = Hekkingen, KT = Kapp Toscana. Nor = Nordmela. Kolje Formation is shown where it is calculated to be, but seismic mapping were not possible. MT = Middle Triassic, 2 different lithostratigraphy because of erosional border. Base = Base of Permian. Orange line indicate projected wellbore position, the well is perpendicular ~2,5 km east from the seismic (Fig. 11), and ends at the calculated 2375ms, see Fig. 19 for log. Lines 1. and 2. indicate the two major faults in the area, (Fig. 21). Black polygon with yellow line indicate the seismic line's position in the survey. Structural smoothed with X, Y & Z at 1.5. Inline nr. 6964. See Fig. 20 to see the interpretations of the horizons.

4.1.2 Base

This lithology is not present in the wells; therefore it is no exact result to show to. However, if Fig. 17 is compared to Fig. 13, then the basement should be of near Permian age.

The base have parallel to sub-parallel, with some vertical offset from west to east, internal reflector configuration (Fig. 18). The reflector continuity is high with high to moderate amplitude from bottom to top, with a more disturbed area in the east. However, the reflections are traceable through the more chaotic zone as well. The transitional zone between base Permian and the middle Triassic, ~400-800 ms TWT above the base, is unconformable and consist of chaotic and at times untraceable reflections (Fig. 18).

4.1.3 Middle Triassic.

This lithology is, also, not present in the wells, therefore there is no exact result to show to. However, if Fig. 17 is compared to Fig. 13, then the marked area should be of intra-middle Triassic.

The middle-Triassic have parallel to sub-parallel internal reflector configuration (Fig. 18). The reflector continuity is semi-continuous with low to moderate amplitude from bottom to the top (Fig. 18).

4.1.4 Kapp Toscana Group.

The deepest, identified, lithology in the study is the Kapp Toscana Group (Fig. 17). In the well log of 7119/12-1 it is located at a TVD of 2658m, and continues until the end of the well at 3000mbsl. In the study area the Stø - and Nordmela Formations exist. From the starting interpretation point (Fig. 17-orange line) this group is the only below URU which is mapped in the whole survey (Fig. 20). As such it is mapped at very different depths from the highest point at ~500 ms TWT to the deepest at ~3000 ms TWT (Fig. 20).

In the FP section of the survey (Fig. 11): the Kapp Toscana Group have parallel to sub-parallel internal reflector configuration. The reflector continuity is high to moderate, with some lateral discontinuities where it seem the layers have vertical offset. The reflectors also dip downwards from east to west. The amplitudes are moderate.

In the Hammerfest Basin (HB) section of the survey (Fig. 11): the group have sub-parallel and wavy internal reflector configuration (Fig. 17). The reflector continuity is semi-continuous to high from bottom to the top. The group dip downwards with low to high continuity from west to east. The amplitudes are moderate to high, and may be due to coal layers being present in the group (see 2.3.7 Kapp Toscana Group.)(Fig. 17).

In the Ringvassøy Loppa Fault Complex (RLFC) (Fig. 11): the group have sub-parallel internal reflector configuration. The reflector continuity is semi-continuous to low continuity from bottom to the top of the group (Fig. 17). The amplitudes are low to moderate (Fig. 17).

The group have two sections of lateral discontinuity zones labelled Tromsø Finnmark Fault Complex (TFFC) and RLFC (see fault 1. & 2. in Fig. 17).

The gamma ray value is chaotic within the Stø formation (Fig. 19); the only formation present in the well log, with values from ~10 and up to ~120 API, the low API value is probably due to the coal. Velocity is high with an average of ~4600 m/s while the group's densities vary between 2500 to 2600 kg/m^3, which is very steady compared to the other groups. The low API is probably because of the coal layers in the group, both the high and stable velocity and density, which increase with depth, could be because diagenesis have started to act on the sediments (Nichols, 2009; Rider, 2011).

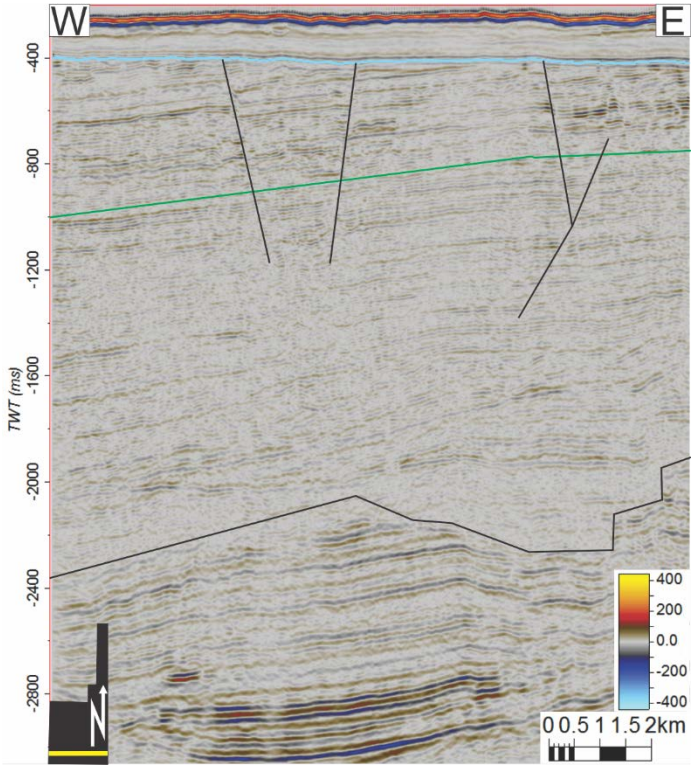

Fig. 18: Seismic line 6092. Black line is top Base. Green line is top middle Triassic. Icy blue line is top Kapp Toscana Group and URU. Above URU is Nordland Group. Black polygon with yellow line indicate seismic line position.

4.1.5 Adventdalen Group.

Adventdalen Group with Kolmule -, Kolje -, Knurr - and Hekkingen Formation are present in the area between ~800ms to ~2200 ms in the south, to ~1200 ms to ~2500 ms in the north of the survey, Fig. 17 & Fig. 20.

The group have parallel to sub-parallel internal reflection configuration (Fig. 17). The continuity is continuous to discontinuous; there are sections with chaotic and dim

reflections (Fig. 19). The amplitude goes from low to moderate increasing from the bottom to the top (Fig. 19). The Adventdalen is not present on the Finnmark Platform (FP) section of the survey and is dipping from downwards south to north.

The Adventdalen Group contains three different formations in the well log and is in total 1600m thick (Fig. 19). The group's well log have visual differences per formation (Fig. 19). The gamma ray intensity is very diverse and goes from ~30 to ~110 API. Velocity is relatively high ~2900 m/s while the group's densities vary between ~1400 to ~2500 kg/m^3 (Fig. 19). The diversity in the log is explained in the description of the group; it is very diverse with shale and claystone being dominant. The low API should be the dolomite in the group, and the high API should indicate shale. The high density should be the dolomite, and the low should be shale (Rider, 2011).

4.1.6 Nygrunnen Group.

Nygrunnen Group or Kveite Formation is positioned between ~800 to ~1200 ms TWT and is only present in RLFC (Fig. 11 & Fig. 17).

The group have a sub-parallel to hummocky internal reflection configuration (Fig. 17). The group is low continuous to discontinuous, i.e. low continuity, but with many lateral discontinuities (Fig. 17). There are zones with discontinuous and un-traceable reflectors (Fig. 17). The amplitudes are low to moderate. The group's middle section, ~900 to ~1000 ms TWT, has moderate amplitude, which may be due to high calc/limestone amount (Fig. 17) (Ostanin et al., 2012).

The gamma ray intensity of the group goes from ~30 to ~60 API increasing downward with two obvious spikes. Densities vary between ~1500 to ~2000 kg/m^3 (Fig. 19). The velocity is goes from ~2700 to ~3000 m/s upwards. As mentioned, it should be mostly claystone with thin interlaying limestone in the group. The low API should be the limestone and the low density should be the clay (Rider, 2011).

4.1.7 Sotbakken Group.

Sotbakken Group, or Torsk Formation is positioned between ~450ms to ~800 ms in the seismic (Fig. 17). The formation declines from 420 in the south to the lowest point of 560 ms in the north (Fig. 20). The group's internal reflection configuration is from parallel, sub-parallel (Fig. 17). The group is continuous, but have lateral disrupted and chaotic reflector continuity, and the amplitude of the group is low to moderate (Fig. 17). From the well log, the group shows an increasing gamma ray intensity going from ~24 to settling on ~40 API with a visible high variability section at ~500 - ~600 TVD, with an average density of ~2100kg/m^3, note that the density log start at 590 TVD (Fig. 19). The velocity starts at ~1500 m/s and goes up to ~2350 ms. The low API could be because of the tuff in the group, the higher section of gamma ray, up to 80 API, is probably more shale containing layers and the low density layers are probably claystone (Crain, 2015; Rider, 2011).

4.1.8 Nordland Group

The first formation encountered after the seabed is the Nordland Group, 25m below the seafloor. The group is between ~260 to ~450 ms, Fig. 17, showing a slight downward dipping northwards, top of layer goes from 225 to 295 ms (Fig. 20). Nordland's lower boundary is the upper regional unconformity (URU), 2.1.3 Cenozoic. The internal reflection configuration is sub-parallel to mounded, with semi-continuous reflector continuity. The amplitude is low, excluding URU and the Seafloor (Fig. 17). From the well log, the group shows an average gamma ray of ~45 API with an average velocity of 1500 m/s (Table 1 &Fig. 19). Low-medium gamma ray is to be expected with sandstone. Being so close to the seafloor it should be quite porous where the pores are filled with seawater making the velocity ~1500 m/s (Crain, 2015; Rider, 2011).

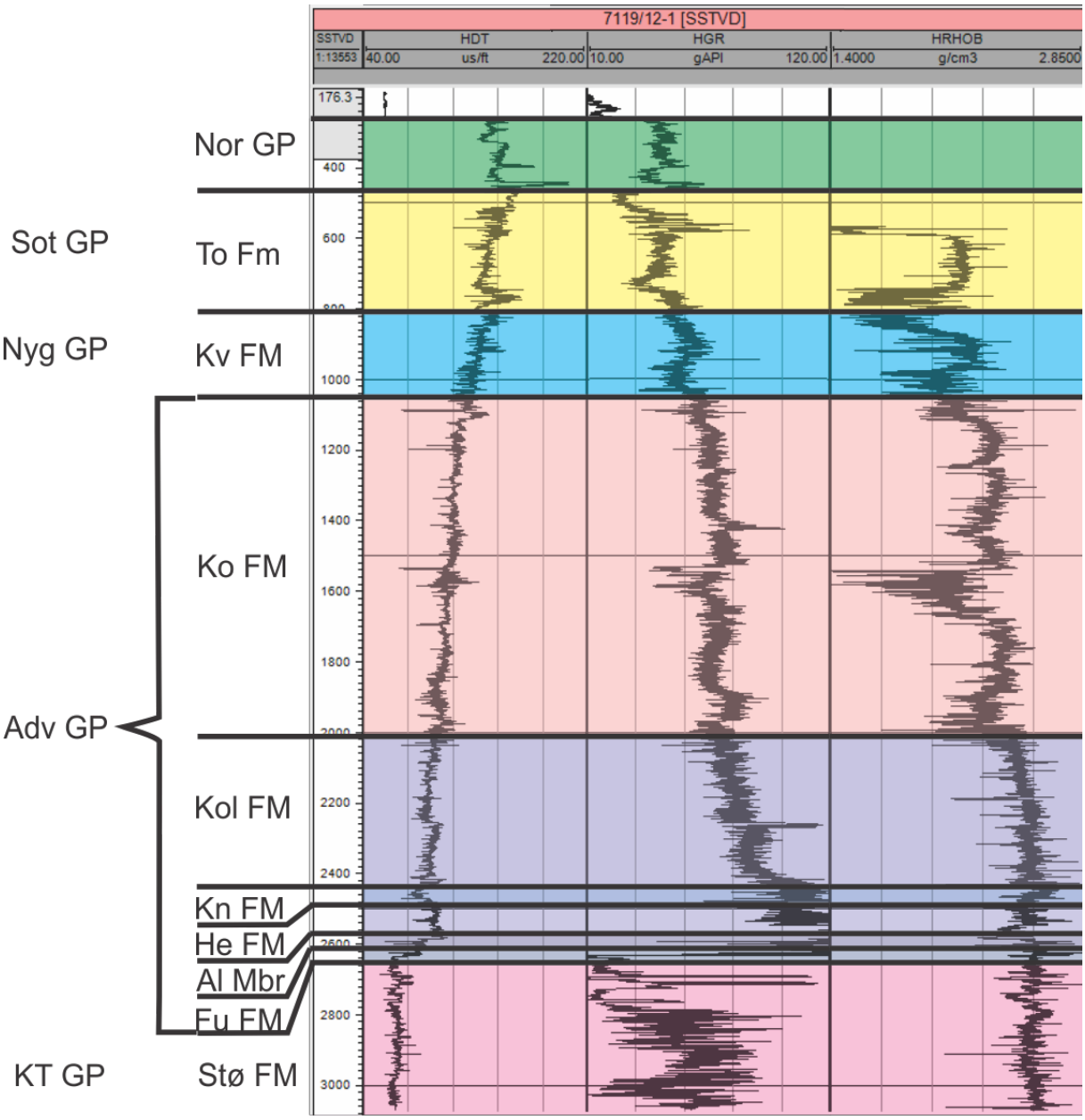

Fig. 19: Well log from 7119/12-1. The different formation is indicated with its own colour. GP = group, FM = formation, No = Nordland, S = Sotbakken, To = Torsk, Nyg = Nygrunnen, Kv = Kveite, Ad = Adventdalen, Ko = Kolmul, Kol = Kolje, Kn = Knurr, He = Hekkingen with Krill member, Al = Alge Member, Fu = Fuglen Formation, KT = Kapp Toscana, Stø formation. Table 1 were used to position the lithostratigraphy. In Fig. 17, the different lithologies are mapped vertically and in Fig. 20 the groups are mapped laterally.

Because of the extensive faulting in the study area the stratigraphy is complex and difficult to map. The different lithostratigraphic units vary in depth, thickness and vertical positioning, with a general downwards trend northwards. The fault zone of Tromsø-Finnmark Fault Complex have also a great throw in the area. Altogether, this made the mapping of the different formations difficult (Fig. 20).

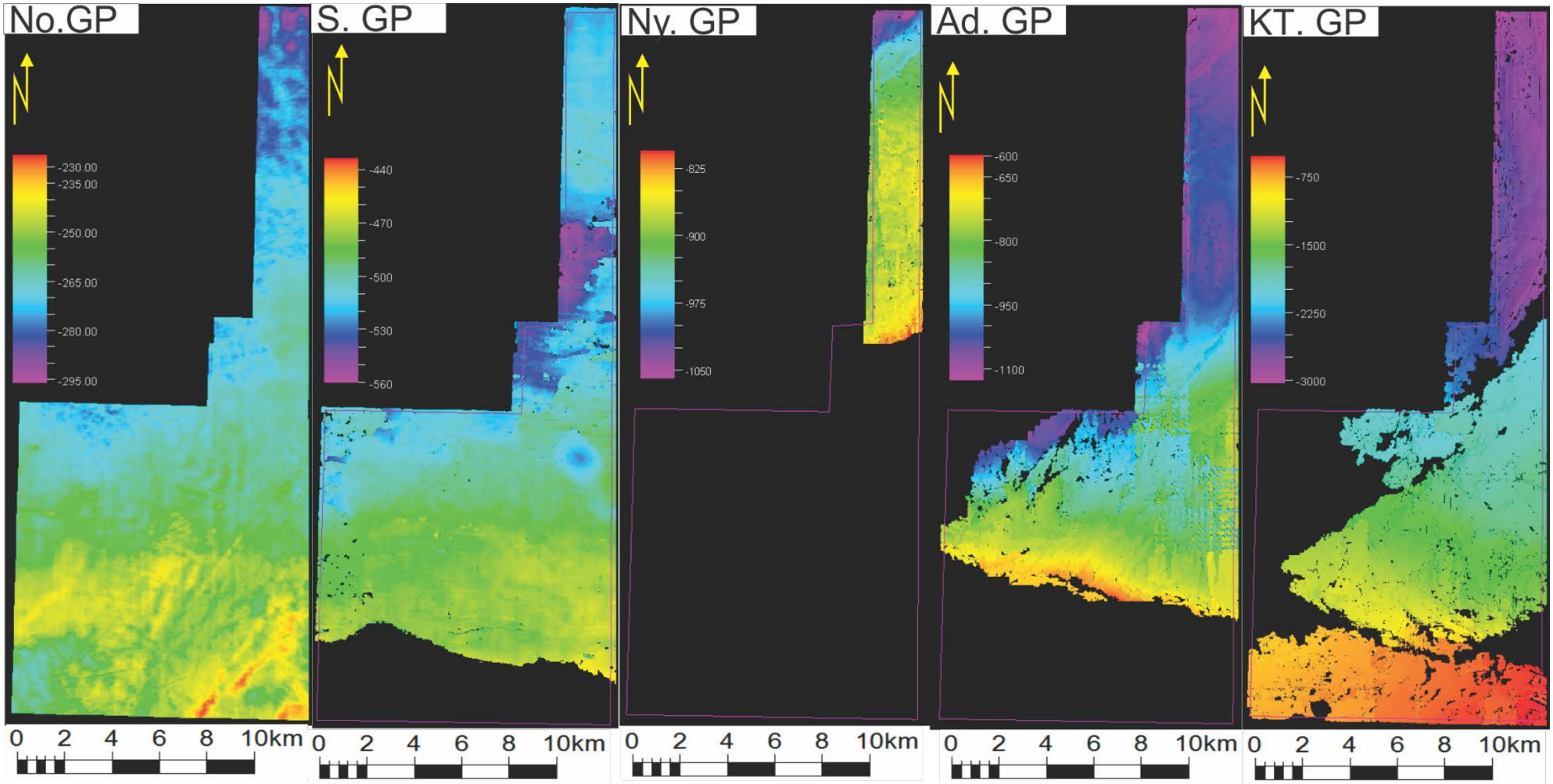

Fig. 20: The seismic interpretation of the top of the different lithostratigraphy groups. See Fig. 17 for location in the seismic. GP = Group, No. = Nordland, S = Sotbakken, Ny = Nygrunnen, Ad = Adventdalen & KP = Kapp Toscana.

4.2 Faults.

As mentioned in Chapter 2, the study area has undergone tectonic activity, which resulted in fault developments. This is further prefaced with two of the major structural elements in the area named “Fault Complex” – Ringvassøy Loppa Fault Complex and Tromsø Finnmark Fault Complex.

In the theory it is mentioned: “In the seismic, the fault itself is often too narrow to be visualized on the seismic data; a vertical section of lateral discontinuous reflectors with vertical offset, to a “matching” reflector, are therefore interpreted as faults in the dataset”. Further the faults are presented in four different categories differentiated by colour, which depend on the different lithostratigraphic units affected (Fig. 21). Green coloured faults are an exception to this and represents the faults on the Finnmark Platform.

The acoustic masking present in some of the faults made the interpretation challenging. This lead to a confidence scale of 1 to 3 (Fig. 21). By confidence, it is meant the amount of certainty that the fault is present and similarity to the interpretation mapped. The faults were given a level of confidence depending on different factors: Chaotic seismic reflectors, indication of throw, indication of fault in variance map, number of seismic lines the fault is present in. Especially the amount of chaos in parts of the survey made the interpretation work on faults difficult. Level 3 confidence is given when it is high certainty that the fault is interpreted correct and a level 1 confidence when the interpretation is uncertain.

Furthermore, when mapped it is visible that the general direction of the faults differ (5-Fig. 21). The orange stippled coloured line indicate the projected border where the faults change direction from WNW – ESE (Fig. 21). Just to the north of the green stippled line, the faults change direction from NE – SW to N-S further to the north (Fig. 21). This change in direction coalign and indicate the borders between the structural elements (Fig. 12). The faults are also given a number between 1-3 for confidence, 1 low and 3 high, based on their interpretation and visibility in the seismic (Fig. 21). This was done because chaotic reflection zones in the seismic make the interpretation sometimes difficult and less confident.

4.2.1 Deep-seated faults.

The deepest faults in the area starts beneath 3s TWT of the survey and their roots cannot be documented. The ones located in the TFFC reach up to the URU (yellow coloured Fig. 21), and affect a from 500 ms TWT to the bottom of 3000 ms TWT.

The Kapp Toscana group have two zones of disturbed and chaotic reflections (Fig. 21Fig. 17). One of these chaotic zones are the TFFC, located just north of FP (Fig. 11 & Fig. 21). The vertical offset due to TFFC is from ~400 ms TWT to ~1400 ms TWT, increasing westward (Fig. 21). This vertical offset is probably due to several faults, which together have been categorized as F1.

F2 is in the central-east of the study area, i.e. the border between HB and RLFC (Fig. 21). This is not as problematic as the TFFC fault zone due to much less chaotic reflections. Here, the vertically displacement of the Stø formation is ~550 ms TWT (Fig. 21). Further up in the seismic record, the F2's throw decreases, e.g. the affected Knurr formation has a throw of only ~100ms and, higher up, the affected Kolje Formation has a throw of only ~50ms. Note, the exact location where the fault terminates at the base is difficult to interpret due to chaotic reflections, but it may be at ~800 ms TWT (Fig. 21).

The throw of Fault 2 increase with depth suggest that it has been reactivated multiple times. Kolmule Formation seem to be the highest formation affected by Fault 2, i.e. Fault 2 have not been active after Albian – middle Cretaceous (Fig. 20).

Fault 1. does not affect URU, but the glacial cycles have eroded the Finnmark Platform to an effect that only the Kapp Toscana Group – Middle Jurassic is present (Fig. 13 & Fig. 21). The faults connected to Fault 1. does not affect the Adventdalen Group, i.e. no indications of activity after Middle Jurassic (Fig. 21).

In summary, the faults F1 & F2. (Fig. 21) are both normal fault zones with the hanging wall to the north of the fault zone. Both can also be traced throughout the survey.

4.2.2 Middle-seated faults.

The middle seated-faults are categorized with two colours: Magenta and pink, and will be described in two following sections.

Starting with the magenta coloured, they are the deepest faults and start at ~2500 ms TWT. They occur so far north in the study area that they are located within the RLFC. They affect the Stø Formation, but not the Nordmela formation (Fig. 21). The exact termination depth of the magenta coloured faults is difficult to determine because of the weak and at times chaotic reflections within the Kolmule Formation (Fig. 21). Whereas the deeper-seated faults show varying throws these middle seated faults are more constant with a throw of ~100-200 ms TWT (Fig. 21).

The middle-seated faults have two main orientations, which are NE-SW and NNE-SSW, but the majority shows a NE-SW orientation (Fig. 21-5). They are interpreted as normal faults, with the hanging wall on the north side of the fault.

The magenta coloured ones seem to affect down to Stø Formation and up the border of Adventdalen – and Nygrunnen Group (Fig. 21). Which means they were active post-Adventdalen Group and either pre-Nygrunnen Group or Nygrunnen were simply not reached. The magenta coloured faults (Fig. 21) have the same orientation as the deep-seated faults of RLFC, e.g. Fault 2, or a slightly more N-NE-S-SW orientation, which is typical for the faults in RLFC (Gabrielsen, 1984; Gabrielsen et al., 1990).

The pink coloured middle-seated faults start at an unknown depth outside of the survey. One upper termination is at ~900 ms TWT and the other just below the URU at ~550 ms TWT. The throw is of ~100 ms TWT. The formations affected are the Sotbakken Group down to Kolmule (Fig. 21-1).

The pink coloured ones affect from an unknown depth up to the Kveite – and Sotbakken Formation with an orientation of NE-SW, typical for the RLFC (Gabrielsen, 1984; Gabrielsen et al., 1990). The throw of these faults (Fig. 21) seem to be constant, i.e. no indication of reactivation. The northernmost of the two affect Sotbakken formation, so the fault was active post-Sotbakken formation, but not after URU. This makes the northernmost, of the two, pink fault to be the fault that affect the youngest lithology.

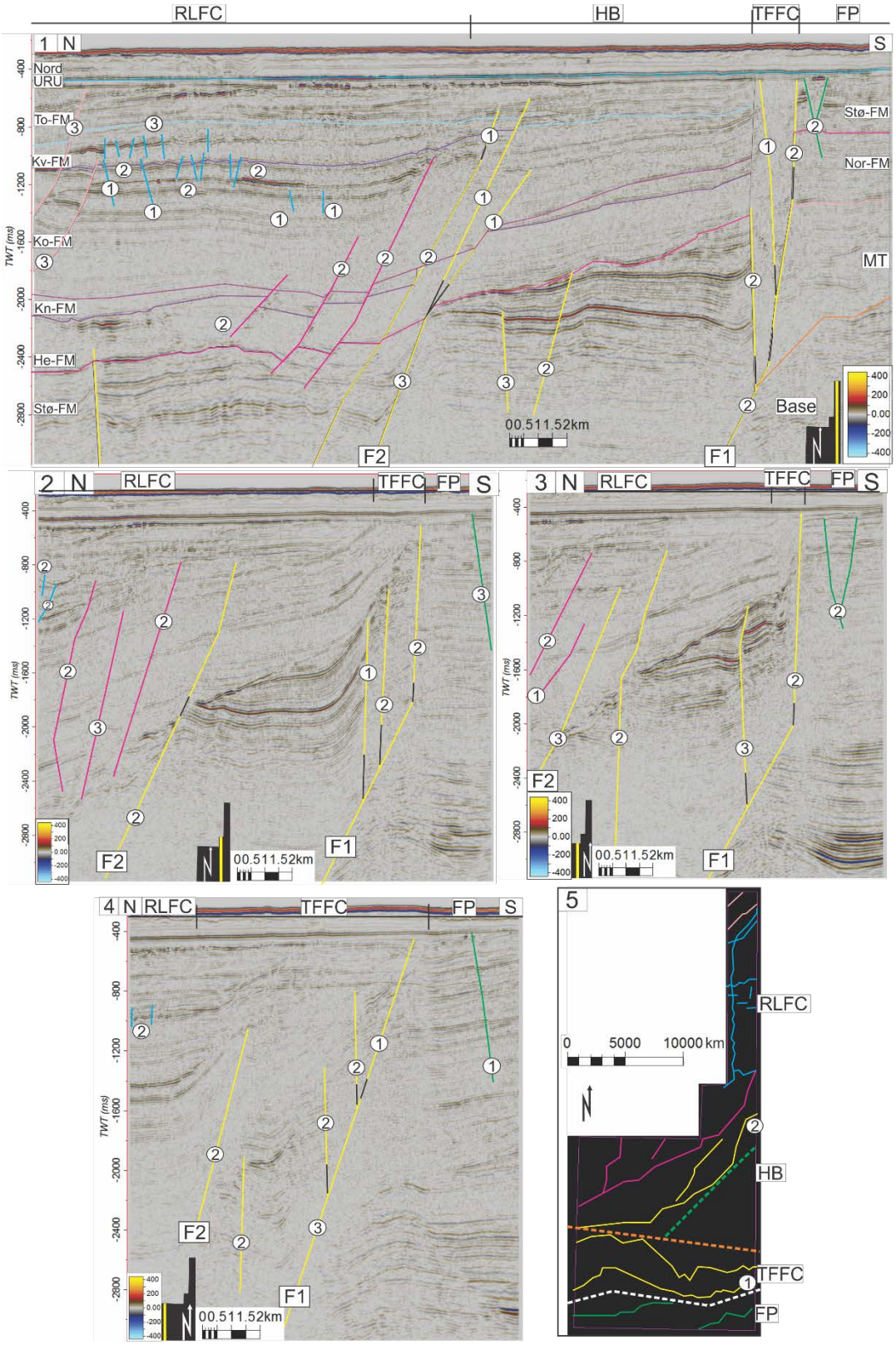

Fig. 21: Picture 1-4 Faults indicated by coloured lines: yellow, green, pink, blue and magenta. Numbers 1-3 given to fault sections/sections to indicate confidence. Black coloured connections are used to indicate faults interpret as result of reactivation. F1 and F2 are two faults present in the whole survey. Yellow line in the black polygon in picture 1-4 indicate the position of the seismic line in the survey. Picture nr.5: The faults are mapped and coloured as given in picture 1-4. Line 1. & 2. indicate the faults F1 & F2 (Fig. 17). In picture 1. the different lithological borders are also mapped, abbreviations in Fig. 17. Inlines used: 6981, 7198, 7430 & 7788 picture 1-4 respectively.

4.2.3 Shallow-seated faults.

In the FP part (Fig. 11) there are some faults, which are coloured green (Fig. 21). Though these are shallow faults in the seismic, they affect the Triassic, Kapp Toscana group and the Middle Triassic. Their orientation is W-E to WSW-ENE and they start at ~1500 ms TWT and terminate at the top of Stø formation (Fig. 17).

The blue coloured shallow-seated faults can be identified in the seismic line with some confidence and start at ~1400ms TWT and terminate at ~1050 ms TWT, i.e. the affected formations are Kolmule – Kveite (Fig. 21). The longest fault is ~400 ms TWT from start to termination, but most have a throw from ~20 to ~100 ms TWT. The faults have a varying orientation of N-S, NE-SW and NW-SE (Fig. 21). These faults seem to be normal faults.

The blue coloured faults can be further categorized into two groups: Located in Nygrunnen Group at ~900 ms TWT and located in Advent Group - Kolmule Formation at ~ 1100 ms TWT. The faults located in Nygrunnen at ~800 - ~1000 ms TWT seem to have less throw, 10-50 ms TWT, but similar orientation as the blue coloured faults in the Adventdalen group (Fig. 21 & Fig. 22).

From the variance slice at -912 ms TWT is seem that the faults in Kolmule Formation are not tectonic faults, but polygonal faults (Fig. 22). The fault network together have the characteristically “honeycomb” intersecting structure pattern. Further observations that support this interpretation are that: The faults have a small throw 10-50 ms TWT and they are normal faults and is in a fine-sediment formation – Kveite / Kviting Formation.

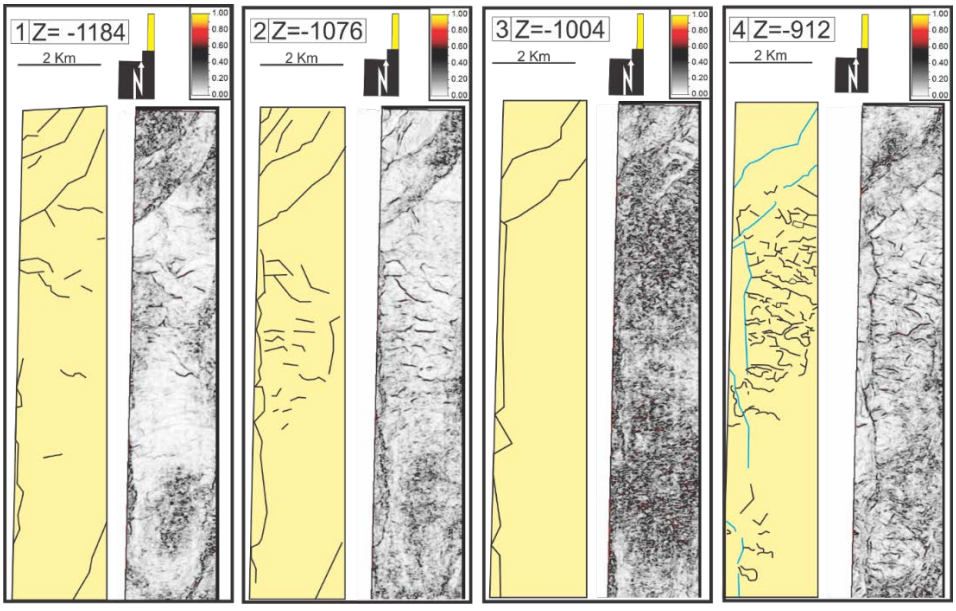

Fig. 22: Variance map of time slices indicated in Fig. 24. The yellow Fig. in the pictures are faults indicated from the variance map. The amount of faults increase from picture 1. to 2. Picture 3: The amount of variance is at the most, near impossible to see faults. Picture 4: More faults are present, blue lines indicate faults also visible on 1-3. With a criss-cross pattern. Z is depth in ms TWT

4.3 Fluid Flow Features.

The survey have several indications of interpret fluid flow features: gas pipes and gas chimneys and seabed depressions. The most notable is presented here to give a representative picture of the study area, i.e. survey ST0825.

4.3.1 Gas Pipes.

There are many lateral disturbances, which break the seismic and seemingly goes further vertically in the seismic. They have no vertical offset on the layers and the reflector is often continuous, less than 200m wide, the features are often close to enhanced reflectors and, sometimes, sub-circular depressions. Features with these characteristic features are interpret as gas pipes.

Gas pipes can be found in the area and some characteristic features will be shown here. They all share some similar characteristics. Most terminate just below URU, with exceptions (Fig. 24, Fig. 25 & Fig. 26). The interpret gas pipes vary between 20 and 80m wide in N-S and E-W direction, i.e. circular, the distance tool in Petrel is used to measure this. There are more gas pipes in the survey area; however, this section will present the characteristic features and their average appearance to give a representative picture of the area.

The gas pipe in Fig. 23, is typical for the survey. Does not break through URU, as best visible in the variance picture (Fig. 23-2). The gas pipe is at its widest ~80m, starts in Adventdalen Group ~1600 ms TWT and terminates just below the URU at ~450 ms TWT showing a total length of ~1000ms TWT close to enhanced reflectors.

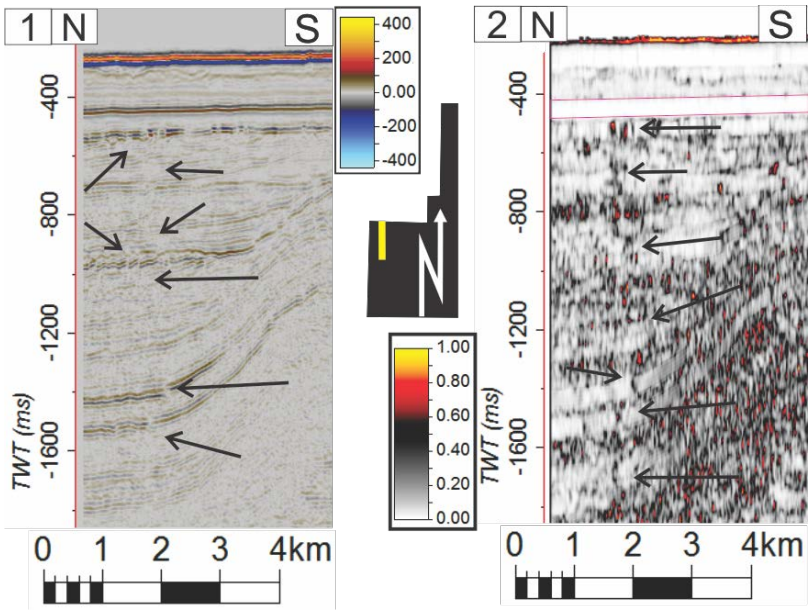

Fig. 23: Gas pipe shown in a seismic picture and in a variance attribute. Inline: 7780, indicated as yellow line on black polygon -survey. In picture 1. black arrows are used to point at local dim zone. In picture 2. the black arrows indicated the same feature as in picture 1. In picture 2, the pink square indicate URU.

In the northern part of the survey, there are many gas pipes in general, inline 7017 were chosen as a representative for this observation (Fig. 24). The gas pipes in this area seem to originate from ~1300 ms TWT, but it is difficult to determine precisely the source because of low amplitude in the reflections of Kolmule Formation (Fig. 21). Some of the gas pipes terminate at URU, but most just below or in the border between the Sotbakken and the Nygrunnen Group, (Fig. 21). The gas pipes of this area are between 30 – 50 m wide.

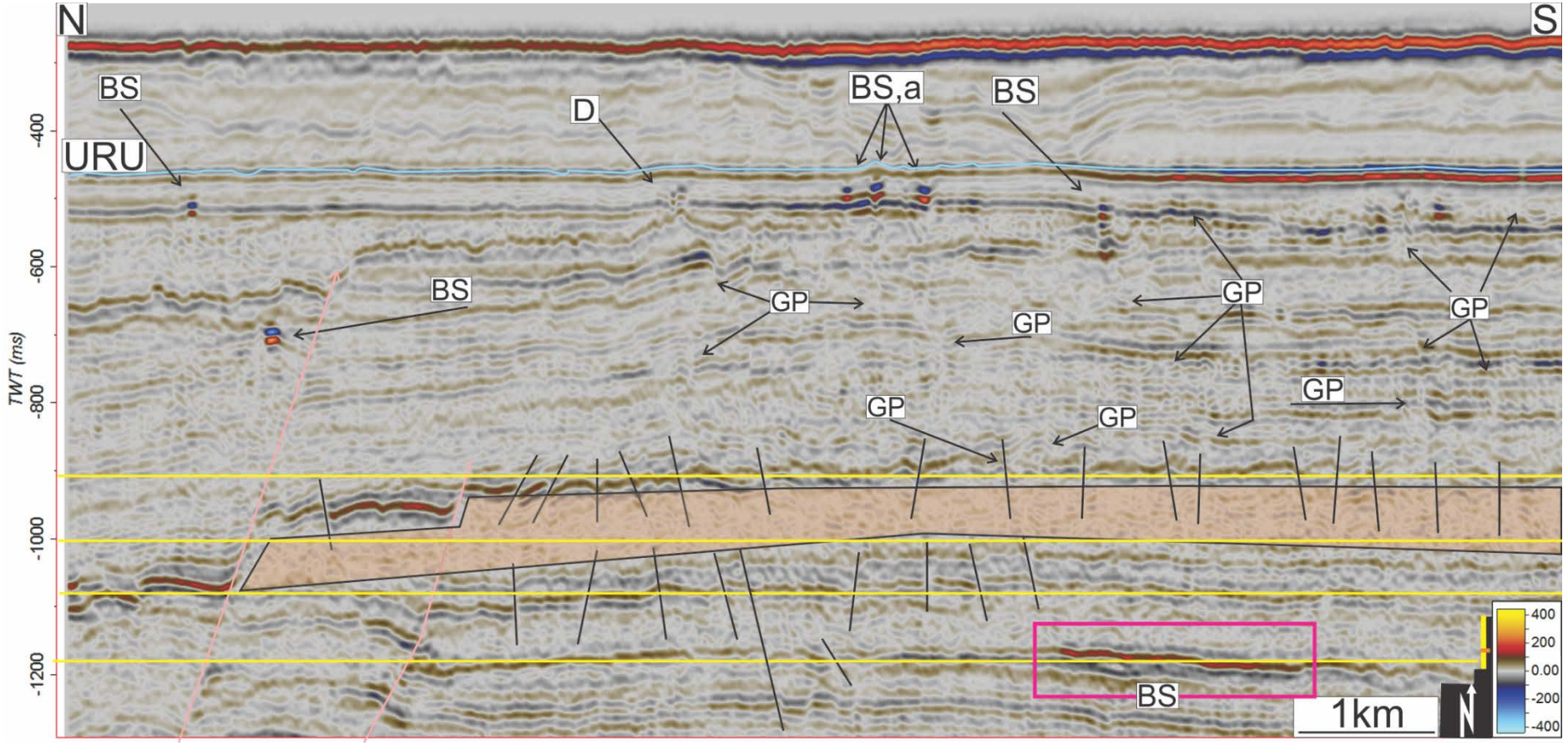

Fig. 24: Fluid flow features in the seismic pointed at by black arrows. Black and pink lines indicate faults. BS = Bright Spot, GP = Gas Pipe, D = Depression, BS,a = Bright spot group A. Marked orange area indicate area of chaotic reflections, see Fig. 22-3. Magenta square indicate an elongated bright spot. Yellow lines indicate the time slices in Fig. 22. Yellow line on black polygon represent the position of the picture in the survey. Inline: 7017.

4.3.2 Morphological Circular to Sub-circular Depressions on the Seabed.

In the survey, on the seabed, there have been identified sub-circular depressions.

The circular depressions are between 70 m and 200 m in diameter and from 11 m to 18 m deep, see Table 2. In the survey, there are mapped sub-circular depressions in the seismic on the seabed horizon (Fig. 25 & Fig. 26).

Number.	*Depth (ms TWT)*	*Avg. diameter (m)*	*Calc. Depth (m)*
1	~7	150	10,5
2	~8,5	70	12,5
3	~7,6	70	11,4
4	~11	200	16,5
5	~12	100	18,0

Table 2: Sub-circular depressions measurements. Depth is measured in milliseconds TWT. Average diameter is in meters. Calculated depth is in meters, 1500m/s is used as speed due to assumed high saltwater content in seabed.

The sub-circular depressions nr. 1, 2, 3 and 5 are positioned vertically above bright spots, where number 2 and 3's bright spot is in close proximity to a fault, ~125 m, note that pockmark number 2 and 3 is positioned on top of the same bright spot. In number 1, 3, 4 and 5 there are also interpret gas pipes in proximity of the depressions. The gas pipe of nr. 1's root is at ~1600ms TWT and is ~40m wide. The gas pipe of nr. 3's root is at ~700 ms TWT and is ~30 m wide. The gas pipe of nr 4's root is at ~800 ms TWT and is ~50 m wide. The gas pipe of nr 5's root is at ~600 ms TWT and is ~45m wide. For depression number 3 the gas pipe is visible from the bright spot to the depression, through the URU (3b, Fig. 26). All of the gas pipe's root is located in the Sotbakken Group.

The sub-circular depressions have been within close proximity, maximum 200m, of long narrow, up to 100 m wide, deep furrows in the seabed. These furrow-like erosional marks are interpret to be iceberg scour marks. The depressions themselves does not seem to be made of glacial erosion, since they are near-perfect circular. Due to this observation and the fluid flow features in close proximity these are interpret to be pockmarks.

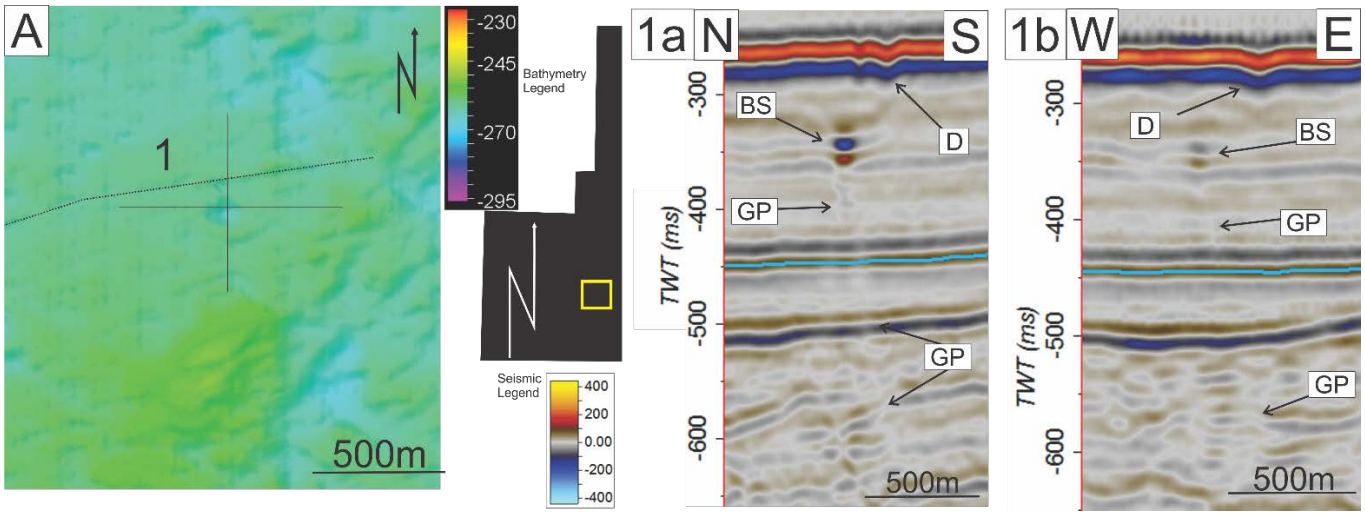

Fig. 25: Sub-circular depression nr.1. Picture A, nr.1 shown in bathymetry, the two lines N-S and E-W indicate the seismic lines. The stippled line indicate an iceberg-scour mark. Picture 1 and 2: D= Depression. BS = bright spot. GP = Gas pipe. Inline: 6979 & Xline: 6829. Vertical exaggeration of 3 is used in picture A. See Fig. 27 of a larger seismic section. Yellow square on black polygon indicate position of picture A.

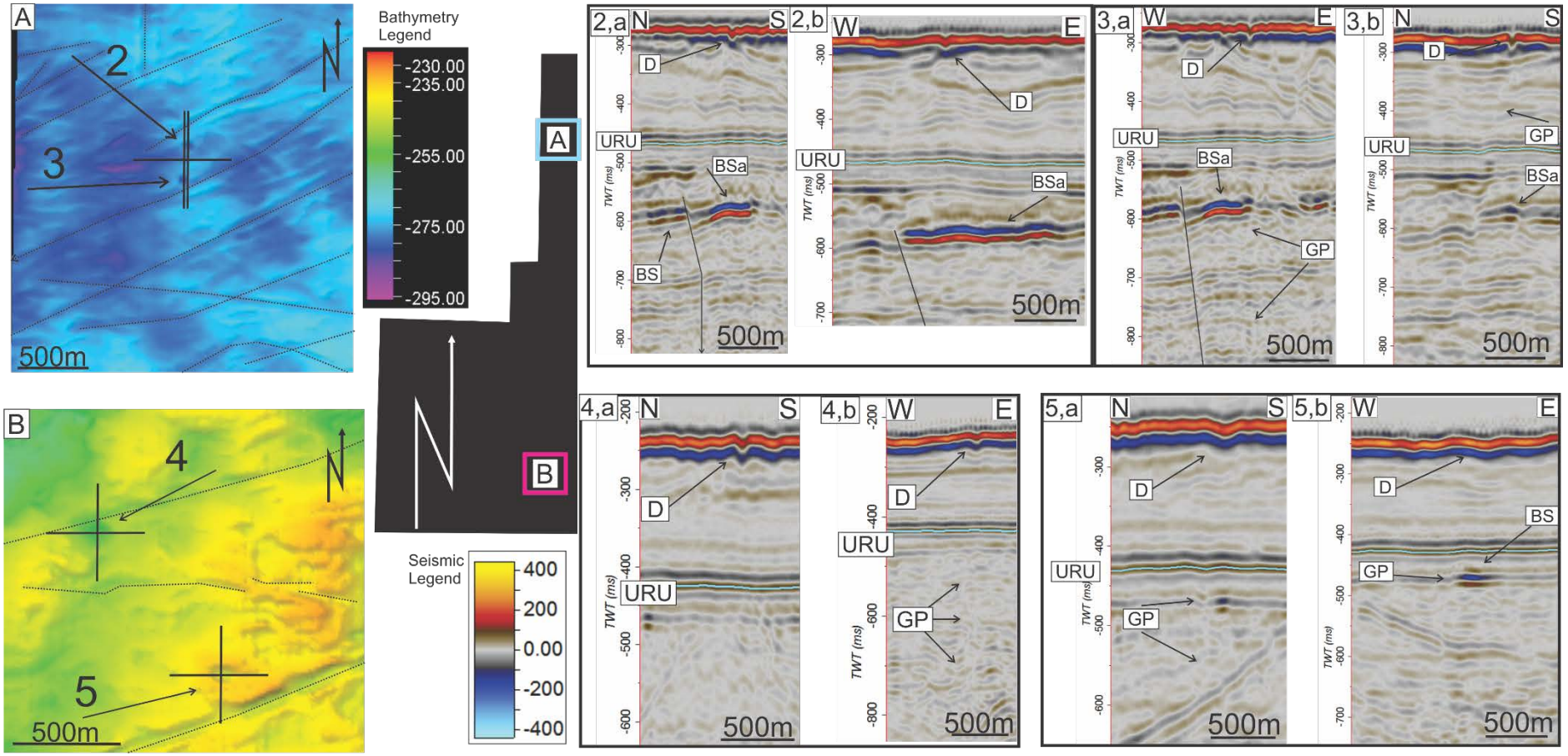

Fig. 26: Sub-circular depression 2-5. Picture A and B is taken with vertical exaggeration of 3 and show the Sub-circular depression at the seabed in a bathymetry map. The stippled lines indicate iceberg ploughmarks and the numbered arrows indicate the position of the pockmark with the same number. The black polygon with coloured squares indicate the position of picture 1 & 2 in the survey; light blue square is picture A and magenta square is picture B. D= Depression. BS = bright spot. GP = Gas pipe. URU = upper regional unconformity. Seismic lines used are: 2-in 6987 xl 7971, 3 in 6989 xl 7954, 4 in 6998 xl 6286 & 5 in 7045 xl 6341.

4.4 Amplitude Anomalies.

Amplitude anomalies have been mapped throughout the survey, both laterally and vertically in the form of enhanced seismic reflectors, bright spots, chaotic discontinuity zone and acoustic masking.

4.4.1 Chaotic reflection zones.

The survey have several areas with chaotic reflection zones. These chaotic reflection zones seem to extend both laterally and vertically, and different in the lithostratigraphies. The zones are identified by their discontinuous and chaotic reflections and lower frequency. Some of the chaotic reflection zones areas terminate at the start of gas pipes with enhanced seismic reflectors; these are interpret as gas chimneys. There are three areas of chaotic reflection zones, which will be presented here Nr. 1-3, shown in the seismic (Fig. 27).

Chaotic reflection zone Nr. 1 seem to have its root at ~1900 ms TWT, which is in the Kolje Formation, and terminate at ~800 ms TWT (Fig. 27). This chaotic reflection zone is at its widest ~1km N-S and >2km E-W, it goes out of the survey. At its termination point, gas pipes start and bright spot group B is located in 185 ms TWT above it (Fig. 24). Note that per the interpretation it is a fault at the chaotic reflection zone's root, this fault function as the chaotic reflection zone southern border (Fig. 27). These observations with and with the zone's funnel-like shape leads to the interpretation that chaotic reflection zone nr.1 is a gas chimney. Gas chimney 1. seem to affect the lithologies beneath Sotbakken Group the most. This can be an indication that the gas flux has decreased after through time. The Sotbakken Group seem to have functioned as a weak seal. There are gas pipes present from ~800 ms TWT into bright spot group B located in the Torsk Formation, indicating that there has been migration of hydrocarbons after Torsk Formation were deposited (Fig. 27).

Chaotic reflection zone area Nr. 2, has its root at ~1300 ms TWT, in the Kolmule Formation, and terminates at ~700 ms TWT (Fig. 27). It is at maximum ~1 km wide in N-S and ~1 km wide E-W. This chaotic reflection zone seems too to start in a fault (Fig. 27). These observations with and with the zone's funnel-like shape leads to the interpretation that chaotic reflection zone nr.2 is, also, a gas chimney. But, whereas gas chimney 1. is underneath bright spot group B, gas chimney 2 have no significant bright spots above it. The more chaotic seismic reflections in gas chimney nr.2 stop at ~800 ms TWT where Sotbakken Group is deposited. However, there are gas pipes at the termination and going up to several stronger reflections ~50 ms TWT below URU, seemingly in the same layer as bright spot group B. This re-inforce the conclusion that Torsk were deposited before the gas chimneys were active.

Chaotic reflection zone Nr.3, is the greatest one, with a high variance in distribution (Fig. 27). This chaotic reflection zone is the only one, which is in two structural elements, namely FP and TFFC. It seem to root at ~2000 ms TWT and terminates at ~500 ms TWT (Fig. 27). At its widest it is ~3 km N-S and up to 5 km E-W. Connected with chaotic reflection zone Nr. 3 is chaotic reflection zone Nr 5. Chaotic reflection zone Nr.5 starts ~2350 ms TWT and terminates ~800 ms TWT. It is at its widest ~5 km E-W and ~2.4 km N-S.

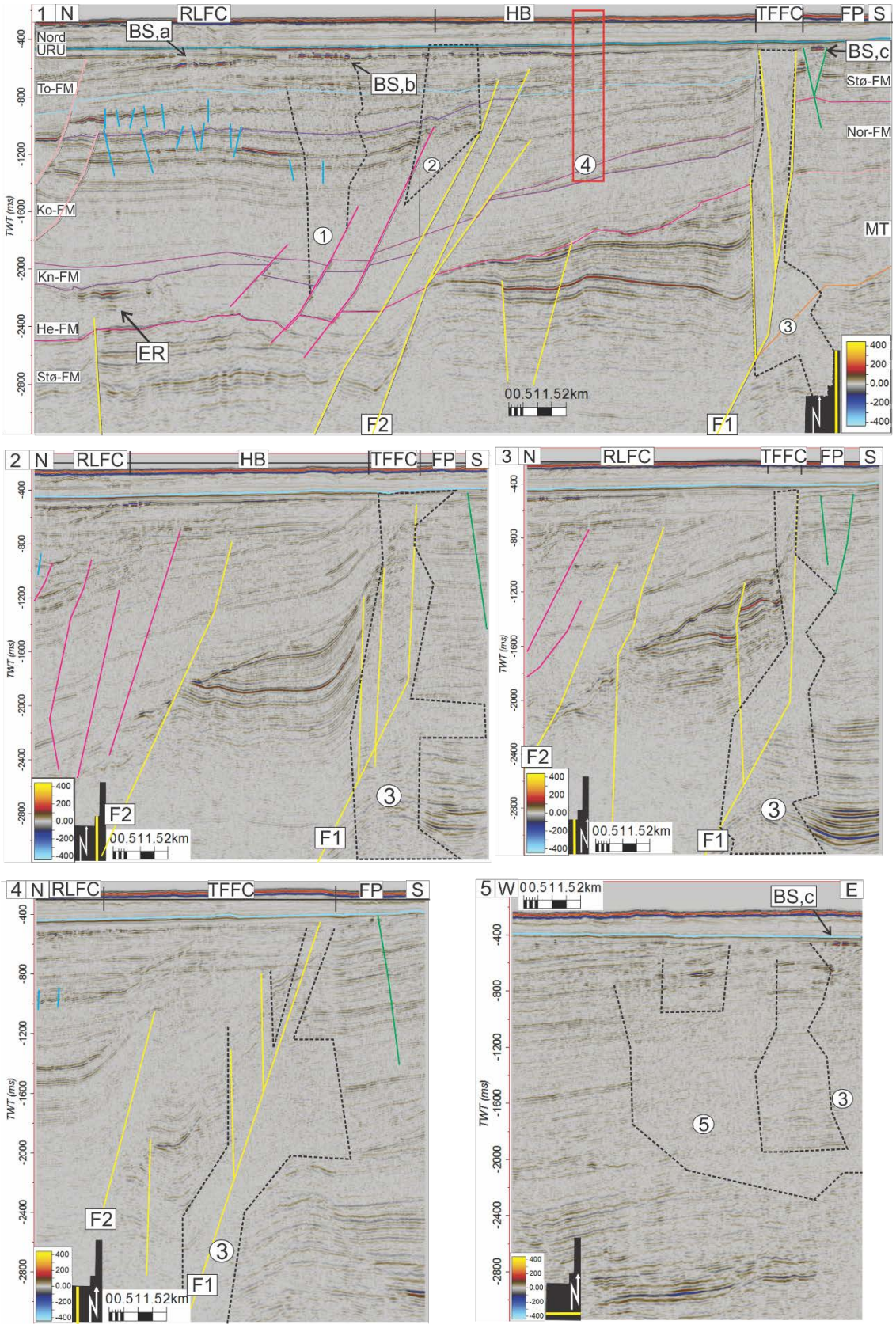

Fig. 27: Noticeable acoustic masking is marked within black stippled lines, and given an identification number 1-5. BS= Bright spot. ER= Enhanced seismic reflector. The coloured lines are the same as used to indicate faults in Fig. 21. In picture 1. the orange square numbered 4. is location of Fig. 25. The yellow line on the black polygon indicate position of the seismic line in the survey. In picture 1. the different lithological borders are also mapped, abbreviations in Fig. 17. Inlines used: 6981, 7198, 7430 & 7788 picture 1-4 respectively, same as in Fig. 21. In picture 5 is Xline 6194.

4.4.2 Enhanced Seismic Reflectors.

There are two types of enhanced seismic reflectors mapped in this survey: the fast-to-slow and slow-to-fast, i.e. fast is positive amplitude and slow is negative amplitude. Most of the enhanced seismic reflectors, in the survey have been identified above ~1500 ms TWT and the amplitude of these does not exceed +/-300 (Fig. 27).

The deepest enhanced seismic reflector mapped is located at -2166 ms TWT in the Knurr Formation (BS,d Fig. 27-1). The shallowest is located at 340 ms TWT (Fig. 25). The biggest enhanced seismic reflector mapped is ~1.5 km long with a thickness of ~15 ms and is located on ~1160 ms TWT, -Kolmule Formation (Fig. 24), it consist of a layer with an amplitude of +170 on top of a layer with amplitude of -135.

Enhanced seismic reflector A (Fig. 27 & Fig. 28) will be described as one group, since the bright spots are within one seismic reflector. This group is 2100m N-S and 1200m W-E and 50 ms TWT from topmost point to downmost point, and lies in the Sotbakken Formation, ~200 ms TWT beneath URU.

Enhanced seismic reflector B is ~1000 m N-S and ~800m E-W with amplitude of -260 followed by +80 (BS,b Fig. 27 & Fig. 28), and lies too within the Sotbakken Group.

Enhanced seismic reflector A & B are vertically positioned close at 570 and 520 ms TWT and distributed over an area of ~3,8 and ~5,25 km^2 respectively (Fig. 28). In Sotbakken Group the enhanced seismic reflector vary from amplitude from -320 to -180 with widths of ~60 - 90m (Fig. 24). The enhanced seismic reflector, those above 700 ms TWT in the northern part of the dataset are included in the RMS map (Fig. 28).

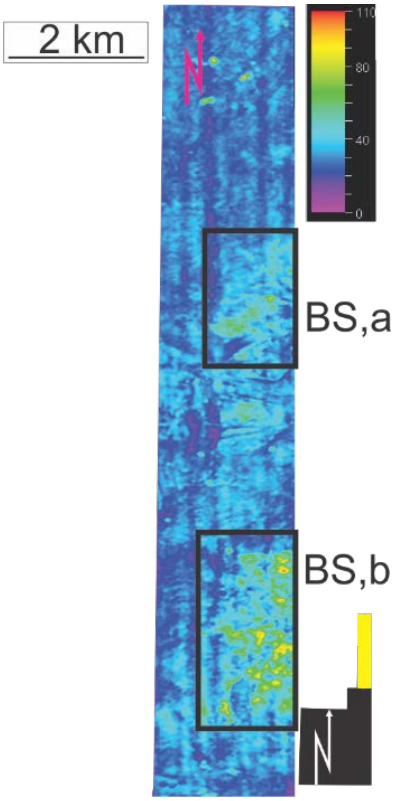

Fig. 28: RMS map of 500-700 ms. With BS,a and b indicated on surface.

Enhanced seismic reflector C, lies between the two faults (Fig. 27). This is enhanced seismic reflector at maximum ~900m N-S and ~1000m E-W at 460 ms TWT, and have acoustic masking beneath (BS,c Fig. 27-5).

Enhanced seismic reflectors are also mapped above URU, underneath the sub-circular depressions (Fig. 26 picture 2a,b, 3a,b and 5,b). The enhanced seismic reflector in picture 2 and 3 is the BS,a (Fig. 27). The enhanced seismic reflector in picture 5. is ~140m N-S and ~300m E-W, with an amplitude with -130 and +100 (Fig. 26). These enhanced seismic reflector are located in close proximity to either a fault, a gas pipe or both – within 500m.

The enhanced seismic reflectors groups A, B & C are interpret as bright spots. Since they are all within close proximity to other fluid features, gas pipes or pockmarks.

5 Discussion.

The result chapter presented findings and interpretations of stratigraphy, faults, fluid flow features with acoustic masking and fluid flow features. This chapter, hopes to integrate these observations to create a wholly representation of the study area

5.1 Fault Networks and Activity.

As written in Chapter 2, the tectonic activity for present-day southwestern Barents Sea can be traced back to early Paleozoic (Doré, 1995; Gabrielsen, 1984). The faults in the study area have a wide age difference and some have probably been reactivated more than once (Basov et al., 2009; Doré, 1995; Gabrielsen, 1984; Gabrielsen et al., 1990).

Aiming to get a better understanding of the tectonic active periods in the survey the faults will be categorized per Gabrielsen (1984) classification system (Table 3).

FIRST CLASS	Basement involved	Regional significance	Reactivated	Separate areas of different tectonic outline
SECOND CLASS	Basement involved	Semi-regional	Reactivated / Not-reactivated	Separate areas of different tectonic outline
THIRD CLASS	Basement detached	Local significance	Not reactivated	Does not separate areas of different tectonic outline

Table 3: Classification of fault systems. The faults are categorized into the different classes dependent on the characteristics presented in the results.

Based on Table 3 and the work presented in the results chapter, the main deep-seated faults, Fault 1 and 2, are First class faults. They are interpret to be reactivated, e.g. several faults connect to one root (Fig. 13 & Black connected faults Fig. 21). They are basement involved and separate areas of different tectonic outline: Fault 1 separate the FP and TFFC and Fault 2 separate TFFC and RLFC.

The Middle-, and the Shallow-seated faults presented in the results are per this classification Third class fault: No signs of reactivation. No basement involved and have only local significance (Table 3).

The shallow seated faults seem to all belong to the Third –class; no basement involvement, local significance, are not interpreted to be reactivated and does not affect areas of different tectonic outline.

The green coloured faults seem to affect below URU and down into lithology of estimated middle Triassic age, making the green coloured faults the faults that affect the oldest lithology (Fig. 21).

Per the different orientation and affected lithostratigraphy: F1 and the green coloured faults are part of the TFFC, whereas F2, the pink and the blue faults belong to the RFC, the polygonal fault system excluded (Fig. 21). Due to the affected lithostratigraphy, it seems that TFFC have not been active post-Adventdalen Group - ~Upper Cretaceous. Gabrielsen et. al. (1990) and Gabrielsen (1984) state that TFFC have been active until Eocene. There is no indications of this in the survey, which neither speak for nor against Gabrielsen's statement since the study area contain only a minute part of the TFFC.

The deep-seated faults of RLFC affect from below they dataset and terminate top of Adventdalen Group. From this these faults have last been active after the Adventdalen were deposited, Upper Cretaceous. The middle- and shallow-seated faults in the RLFC have similar dip and orientation to F2, but not as deep initiation.. With both Adventdalen -, Nygrunnen – and Sotbakken group being affected by the middle seated faults: these faults may be due to North Atlantic rifting – the subsidising of Hammerfest – and Tromsø Basin in Paleogene (Basov et al., 2009; Henriksen, Bjornseth, et al., 2011). Gabrielsen et al. (1990) and Gabrielsen (1984), state that the RLFC have been active from mid Jurassic and reactivated in the Late Cretaceous and Cenozoic, which coincide with the affected lithologies by the faults in the study area.

The polygonal fault system described and interpret is located in the same formation, Kveite Formation, as the polygonal fault systems Ostanin et al (2012) mapped and described in HB, indicating that the Kveite Formation is prone to polygonal faulting. Ostanin et al (2012) goes further and conclude that the polygonal fault system are of Campanian age, since polygonal faults are believed to develop as the formation is deposited or shortly thereafter (Berndt et al., 2003; Watterson et al., 2000).

5.2 Fluid Migration and Accumulation.

In the survey, many features suggest fluid migration and accumulation. Typical are the acoustic masking along faults and beneath bright spots and gas pipes which indicate fluid migration, e.g. Ligtenberg et al., (2003), Løseth et al (2009) & Vadakkepuliyambatta et al (2015). The bright spots in the Torsk Formation – Sotbakken Group have been interpret to be shallow gas accumulations of other studies: e.g. Arvo (2014), Edvardsen (2015) and Ostanin et al, (2012).

The study area contain both the Stø - and Nordmela Formations. These two formations have shown signs of hydrocarbons around the survey: wellbore 7119/12-1, 7019/1-1 and 7119/9-1 (NPD, 2016b). The Snøhvit production unit's fields are also producing hydrocarbons, gas, in the HB ~30km NE of the study area from reservoirs in the Stø – and Nordmela Formations (NPD). I.e. there are discoveries around the study area that indicate hydrocarbon presence in the Kapp Toscana Group.

5.2.1 Tromsø Finnmark Fault Complex (TFFC).

The TFFC with interpreted Fault 1. has chaotic seismic reflections, which made the interpretation work difficult. The chaotic seismic reflections are present throughout the whole study area, with varying lateral degree (Fig. 27). However, the only bright spot TFFC is in close proximity with is bright spot C, located in the far east of TFFC (Fig. 27). Bright spot C and the fault beneath it are both located in either the Stø – or Nordmela Formation. Therefore, there is a possibility that the bright spot consists of hydrocarbons that already were in the formation before tectonic activity separated the FP section from the rest and that there has been no migration through the fault. Also, there is no indication of fluid migration in the section of Nordland Group above TFFC. There may be several reasons for this: 1.) Chaotic seismic reflections are because of residual hydrocarbons, which are trapped in the dead-end pores. 2) It may be that the seismic survey is off such poor quality that the acoustic masking is because of the severe faulting activity in the area, making the fault zone indistinguishable on the seismic. 3) The tectonic activity in the area have made the fault zone acoustic homogenous by pulverizing the rock.

There is also none DHI's located on top of TFFC in the Nordland Group, too. Although this can be because there has been too little time to affect this lithology. It would have been an abnormally large fluid feature if the chaotic seismic reflections in TFFC were due to a fluid flux, TFFC is ~12.4 km E-W and 1 km – 3 km N-S, therefore it is believed that the chaotic seismic reflectors are due to tectonic activity, i.e. faulting (Vadakkepuliyambatta, Bünz et al., 2013).

5.2.2 Ringvassøy Loppa Fault Complex (RLFC) & Hammerfest Basin (HB).

Gas chimneys mapped in the survey seem both to have roots in faults. Both of these faults are within the RLFC section of the survey and seems to start in Stø –, Nordmela Formation or deeper in the seismic (Fig. 27 & Fig. 29).

The shallow gas accumulations in the Torsk Formation have fluid features below them in the seismic, gas pipes, polygonal faults, faults and beneath bright spot A and B a gas chimney. Indicating that there have been vertical fluid migration in RLFC. There is mapped faulting in both the Advent – and Nygrunnen Group and a layer with tendencies of chaotic reflections in the bottommost section of Nygrunnen Group (Fig. 24). However, there is not mapped any deeper fluid flow features north of gas chimney nr 1. (Fig. 27).

There is however, mapped polygonal faults below the bright spot group A. Polygonal faults are connected to fluid migration (Berndt et al., 2003; Ostanin et al., 2012; Watterson et al., 2000). The polygonal fault system have gas pipes above them indicating fluid flow from the Nygrunnen Group. These gas pipes terminate beneath bright spots in the Torsk Formation (Fig. 24). From these features is can be said that the polygonal faults partake in the migration of hydrocarbons, which accumulate in Torsk Formation. However, there is no hydrocarbon shows in the well 7119/12-1 from this section – Nygrunnen Group (NPD, 2016b). The chaotic seismic reflections may be due to an erosional or depositional event. Ostanin et al., (2012) concluded that this polygonal fault system provided a possible migration pathway, in HB. With similar characteristics in this survey, the polygonal fault system should have similar effect here (Fig. 29).

5.2.3 Accumulation.

The bright spots in the survey are mostly found in the Torsk Formation – Sotbakken Group, indicating that URU may act as a weak seal above it. Further observations which support this statement is the low amount of fluid flow features that goes through URU (Fig. 29). In the Hammerfest Basin there are also mapped several amplitude anomalies in the Torsk Formation e.g. (Arvo, 2014; Edvardsen, 2015; Ostanin et al., 2012). The Torsk Formation were deposited in the late Paleocene and with very few fluid features above the Torsk Formation, indicating that the Torsk Formation may act as a reservoir with URU acting as a weak seal.

Since the bright spots seem to be parallel to the seafloor, it could be a bottom surface reflector (BSR). BSR is the lowest limit of the gas hydrate stability zone (GHSZ) and the GHSZ is calculated to be 50-900 mbsl calculated by Chand et al., (2008) (Chand, Mienert et al., 2008; Vadakkepuliyambatta et al., 2015). The bright spots seen in Torsk Formation at ~500 – 600 ms TWT (~550 mbsl) are within the GHSZ of (Arvo, 2014; Chand et al., 2008; Edvardsen, 2015; Rajan, Bünz et al., 2013; Vadakkepuliyambatta et al., 2015). This suggest that the bright spots located in the Torsk Formation are gas hydrates. Bright spot group C, located on FP is also located at this depth, indicating that these bright spots may also be gas hydrates (Fig. 29).

The bright spot in the Nordland Group, i.e. above URU, is located above a gas pipe that seem to root at ~1600 ms TWT in Hekkingen Formation - Adventdalen Group

(Fig. 25 & Fig. 27). There is a deep-seated fault even lower in the Kapp Toscana Group (Fig. 27). From this it seems that the hydrocarbon in the bright spot may stem from in the Kapp Toscana Group (Fig. 29). Being located in the Nordland Group it is above the estimated GHSZ, and with no other bright spot found in the group it seems reasonable to conclude that it is not a stratigraphy reason for the bright spot to exist. Since Nordland Group is mainly made up of sand- and claystone the hydrocarbons probably accumulated in a sandstone layer with a claystone layer above, acting as a weak seal. After some time with accumulation in the sandstone layer, the pressure increased enough to pierce through the claystone and through the seafloor (Fig. 29) (Berndt, 2005).

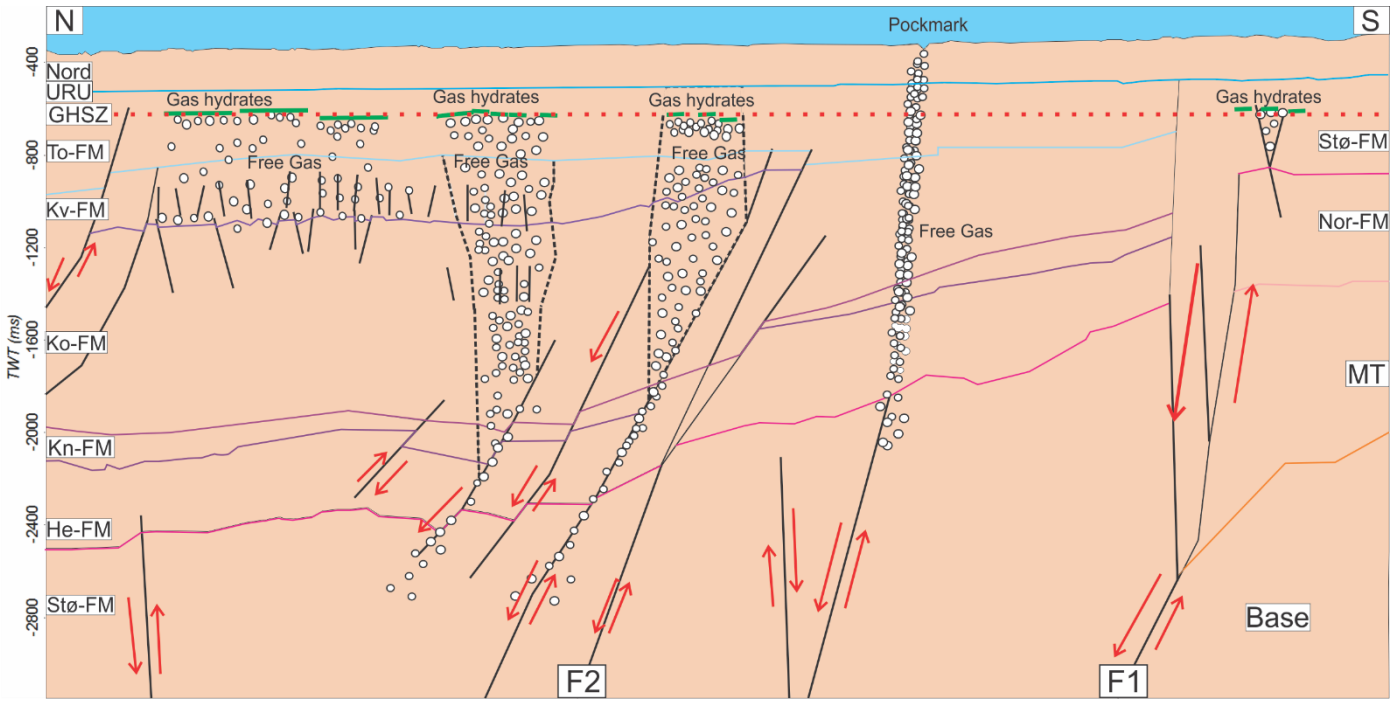

Fig. 29: Sketch of an interpretation of the study area. With the major faults and migration of hydrocarbons. Gas hydrates indicated with green line, with free gas beneath to accentuate the bright spots in Torsk Formation.

5.3 URU and Seabed Fluid Migration and Release.

The Upper Regional Unconformity (URU), were deposited during late Neogene to late Quaternary, and is glacial depositions. Since Sotbakken were deposited late Paleocene to middle Eocene there is approximately 36 million years between the Torsk Formation and Nordland Group.

In the dataset, very few features go through the URU. Only the pockmarks and a bright spot is located in the Nordland Group. (Fig. 25 & Fig. 26). The pockmarks are features that are connected fluid flow (Andreassen et al., 2007; Hovland, 1981; Hovland, 2001; Ligtenberg, 2005; Watterson et al., 2000). Due to their, very, spherical shape, fluid features in close proximity and well documented presence of pockmarks in the south western Barents Sea; there is a very high probability that these depressions are indeed pockmarks and not an anomaly spherical depression from glacial erosion, e.g. (Arvo, 2014; Chand et al., 2008; Chand, Rise et al., 2009; Edvardsen, 2015; Ostanin et al., 2012). If anything the amount of pockmarks in the study area is low, compared to Hammerfest Basin. The reason for this can be that the study area have less hydrocarbons present. It might be that the survey have too small vertical resolution to see smaller pockmarks, the pockmarks mapped have had an average of ~120m diameter with an average depth of ~12m. This is a normal pockmark size, so there is a possibility that there are smaller pockmarks in the area not mapped because of the resolution. Backing up this claim is the work by Rise et al. (2015), most of the pockmarks mapped were 20-50 m wide and 2-5m deep and the biggest were nearly 100m wide and up to 8m deep (Hovland, Gardner et al., 2002; Rise, Bellec et al., 2015). In the areas of the Barents Sea investigated by Rise et al., (2015) there were a typical pockmark density of 150-200 km^2, however the study area of this master thesis were not mapped (Rise et al., 2015).

Faults are also in close proximity to pockmark nr. 2, & 3. The gas may used the faults as a migration pathway and accumulated, visualized in the seismic as bright spots (Ligtenberg, 2005). These pockmarks are the only features mapped that indicate fluid migration after URU in the survey.

6 Summary & Conclusions.

- The faults in the area belong to three different fault systems: TFFC, RLFC and a polygonal fault system.
    - Fault 1. its branches and the green coloured faults on FP, belong to the TFFC.
    - Fault 2. its branches and the middle-seated faults belong to RLFC.
    - The polygonal fault system that is present in the Kolmule - and Kveite Formation have been mapped in Hammerfest Basin by Ostanin et al., (2012).
    - The TFFC have been not affected any lithology younger than Upper Cretaceous, indicating that it has not been active in the study area since.
    - The RLFC have not affected lithology younger than Upper Neogene, indicating that this fault system, too, have not been active post-URU.
        - There is no fault activity mapped above or through URU, i.e. after URU.
- There are indications of fluid migration in the survey ST0825.
    - There are mapped shallow gas accumulations, interpret to be gas hydrates in the Torsk Formation and in the Stø Formation on Finnmark Platform.
- There are evidence of fluid migration post-URU, indicating that there is still active hydrocarbon migration.
    - There are mapped very few pockmarks on the seabed, compared to other areas in the Barents Sea, likely due to low resolution of the dataset.

7 References.

Alcaraz, M., García-Gil, A., Vázquez-Suñé, E., & Velasco, V. (2016). Advection and dispersion heat transport mechanisms in the quantification of shallow geothermal resources and associated environmental impacts. *Science of the Total Environment, 543, Part A*, 536-546. doi:http://dx.doi.org/10.1016/j.scitotenv.2015.11.022

Andreassen, K., Hart, P. E., & MacKay, M. (1997). Amplitude versus offset modeling of the bottom simulating reflection associated with submarine gas hydrates. *Marine Geology, 137 - 1997*, 25-40. doi:10.1016/S0025-3227(96)00076-X

Andreassen, K., Nilssen, E. G., & Ødegaard, C. M. (2007). Analysis of shallow gas and fluid migration within the Plio-Pleistocene sedimentary succession of the SW Barents Sea continental margin using 3D seismic data. *Geo-Marine Letters, 27*(2-4), 155-171. doi:10.1007/s00367-007-0071-5

Andreassen, K., Winsborrow, M. C. M., Bjarnadóttir, L. R., & Rüther, D. C. (2014). Ice stream retreat dynamics inferred from an assemblage of landforms in the northern Barents Sea. *Quaternary Science Reviews, 92*, 246-257. doi:http://dx.doi.org/10.1016/j.quascirev.2013.09.015

Arvo, J. (2014). *Relationship between fluid leakage and faulting along the western and norther margin of the Hammerfest Basin.* (Master Master Thesis), University of Tromsø, Tromsø. Retrieved from http://munin.uit.no/handle/10037/6333

Basov, V. A., Ebbing, J., Gernigon, L., Korchinskaya, M. V., Koren, T., Kosteva, N. V., Kotljar, G. V., Larsson, G. B., Litvinova, T., Negrov, O. B., Olesen, O., Pascal, C., Pchelina, T. M., Petrov, O. V., Petrov, Y. O., Sjulstad, H., Smelror, M., Sobolev, N. N., Vasiliev, V., & Werner, S. C. (2009). *ATLAS - Geological History of the Barents Sea* (M. Smelror, O. V. Petrov, G. B. Larssen, & S. Werner Eds.). Trondheim

Berndt, C. (2005). Focused Fluid Flow in Passive Continental Margins. *Philosophical Tranactions of The Royal Society, 363*, 2855-2871. doi:doi:10.1098/rsta.2005.1666

Berndt, C., Bünz, S., & Mienert, J. (2003). Polygonal fault systems on the mid-Norwegian margin: a long-term source for fluid flow. *Geological Society, London, Special Publications, 216*(1), 283-290. doi:10.1144/gsl.sp.2003.216.01.18

Bjarnadóttir, L. R., Winsborrow, M. C. M., & Andreassen, K. (2014). Deglaciation of the central Barents Sea. *Quaternary Science Reviews, 92*, 208-226. doi:10.1016/j.quascirev.2013.09.012

Bulat, J. (2005). Some considerations on the interpretation of seabed images based on commercial 3D seismic in the Faroe-Shetland Channel. *Basin Research, 17*, 21-42. doi:10.1111/j.1365-2117.2005.00253.x

Burger, H. R., Sheehan, A. F., & Jones, C. H. (2006). *Introduction to applied geophysics, exploring the subsurface*: W.W. Norton&Company

Canty, M. (2014, 07.07.2014). A seismic shift. Retrieved from http://www.maersk.com/en/the-maersk-group/about-us/publications/maersk-post/2014-3/a-seismic-shift

Chand, S., Mienert, J., Andreassen, K., Knies, J., Plassen, L., & Fotland, B. (2008). Gas hydrate stability zone modelling in areas of salt tectonics and pockmarks of the Barents Sea suggests an active hydrocarbon venting system. *Marine and Petroleum Geology, 25*(7), 625-636. doi:http://dx.doi.org/10.1016/j.marpetgeo.2007.10.006

References.

Chand, S., Rise, L., Ottesen, D., Dolan, M. F. J., Bellec, V., & Bøe, R. (2009). Pockmark-like depressions near the Goliat hydrocarbon field, Barents Sea: Morphology and genesis. *Marine and Petroleum Geology, 26*(7), 1035-1042. doi:http://dx.doi.org/10.1016/j.marpetgeo.2008.09.002

Cohen, K. M., Finney, S. C., Gibbard, P. L., & Fan, J.-X. (2013). International Chronostratigraphic Chart. *The ICS International Chronostratigraphic Chart, Eppisode 36*, 5.

Crain, E. R. (2015). Atlas of Log Responses. Retrieved from https://spec2000.net/freepubs/LogResponses.pdf

Dalland, A., Worsley, D., & Ofstad, K. (1988). A lithostratigraphic scheme for the Mesozoic and Cenozoic succession offshore mid- and northern Norway. *Bulletin, 4*, 65.

Doré, A. G. (1995). Barents Sea Geology, Petroleum Resources and Commercial Potential. *Arctic, 48*(3), 15. doi:http://dx.doi.org/10.14430/arctic1243

Edvardsen, A. (2015). *Faulting and the relationship to fluid migration and shallow gas accumulation in the Hammerfest Basin, SW Barents Sea.* (Master), University of Tromsø, Tromsø. Retrieved from http://munin.uit.no/handle/10037/7701

Faleide, J. I., Gudlaugsson, S. T., & Jacquart, G. (1984). Evolution of the western Barents Sea. *Marine and Petroleum Geology, 1*(2), 123-150. doi:http://dx.doi.org/10.1016/0264-8172(84)90082-5

Fishsafe.eu. Seismic Surveys. Retrieved from http://fishsafe.eu/en/offshore-structures/seismic-surveys.aspx

Gabrielsen, R. H. (1984). Long-Lived Fault Zones & Their Influence On The Tectonic Development Of The Southwestern Barents Sea. *Journal of the Geological Society, 141*(JUL), 651-662. doi:10.1144/gsjgs.141.4.0651

Gabrielsen, R. H., Færseth, R. B., Jensen, L. N., Kalheim, J. E., & Riis, F. (1990). *The Barents Sea Region* (82-7257-304-0). Retrieved from

Gudlaugsson, S. T., Faleide, J. I., Johansen, S. E., & Breivik, A. J. (1998). Late Palaeozoic structural development of the South-western Barents Sea. *Marine and Petroleum Geology, 15*(1), 73-102. doi:http://dx.doi.org/10.1016/S0264-8172(97)00048-2

Henriksen, E., Bjornseth, H. M., Hals, T. K., Heide, T., Kiryukhina, T., Klovjan, O. S., Larssen, G. B., Ryseth, A. E., Ronning, K., Sollid, K., & Stoupakova, A. (2011). Uplift and erosion of the greater Barents Sea: impact on prospectivity and petroleum systems. In A. M. Spencer, A. F. Embry, D. L. Gautier, A. V. Stoupakova, & K. Sorensen (Eds.), *Arctic Petroleum Geology* (Vol. 35). Bath: Geological Soc Publishing House.978-1-86239-328-8

Henriksen, E., Bjørnseth, H. M., Hals, T. K., Heide, T., Kiryukhina, T., Kløvjan, O. S., Larssen, G. B., Ryseth, A. E., Rønning, K., Sollid, K., & Stoupakova, A. (2011). Uplift and erosion of the greater Barents Sea: impact on prospectivity and petroleum systems. *Geological Society London Memoirs*(08), 271-281. doi:10.1144/M35.17

Hovland, M. (1981). Characteristics of pockmarks in the Norwegian Trench. *Marine Geology, 39*(1), 103-117. doi:http://dx.doi.org/10.1016/0025-3227(81)90030-X

Hovland, M., Gardner, J. V., & Judd, A. G. (2002). The significance of pockmarks to understanding fluid flow processes and geohazards. *Geofluids, 2*(2), 127-136. doi:10.1046/j.1468-8123.2002.00028.x

Hovland, M., Jensen, S., & Indreiten, T. (2012). Unit pockmarks associated with Lophelia coral reefs off mid-Norway: more evidence of control by "fertilizing" bottom currents. *Geo-Mar Lett, 32*, 545-554. doi:10.1007/s00367-012-0284-0

References.

Hovland, M., & Judd, A. G. (1988). *Seabed Pockmarks and Seepages*. London: Graham and Trotman Inc.

Hovland, M. G., J. V; Judd, A.G. (2001). The significance of pockmarks to understanding fluid flow processes and geohazards. *Geofluids, 2 - 2002*, 127-136.

Judd, A. G., & Hovland, M. (1992). Methane in Marine Sediments The evidence of shallow gas in marine sediments. *Continental Shelf Research, 12*(10), 1081-1095. doi:http://dx.doi.org/10.1016/0278-4343(92)90070-Z

Krooss, B. M., & Leythaeuser, D. (1996). Molecular Diffusion of Light Hydrocarbons in Sedimentary Rocks and its Role in Migration and Dissipation of Natural Gas. *Hydrocarbon migration and its near-surface expressions: AAPG Memoir, 66*, 173-183.

Larssen, G. B., Elvebakk, G., Henriksen, L. B., Kristensen, S.-E., Nilsson, I., Samuelsberg, T. J., Svånå, T. A., Stemmerik, L., & Worsley, D. (2002). Upper Palaeozoic lithostratigraphy of the Southern Norwegian Barents Sea. *NPD Bulletin, 9*, 76.

Ligtenberg, H. (2005). Detection of fluid migration pathways in seismic data: implications for fault seal analysis. *Basin Research, 17*, 141-153. doi:doi: 10.1111/j.1365-2117.2005.00258.x

Ligtenberg, H., & Connolly, D. (2003). Chimney detection and interpretation, revealing sealing qualityof faults, geohazards, charge of and leakage from reservoirs. *Journal of Geochemical Exploration, 78–79*, 385-387. doi:http://dx.doi.org/10.1016/S0375-6742(03)00095-5

Løseth, H., Gading, M., & Wensaas, L. (2009). Hydrocarbon leakage interpreted on seismic data. *Marine and Petroleum Geology, 26*(7), 1304-1319. doi:http://dx.doi.org/10.1016/j.marpetgeo.2008.09.008

Løseth, H., Wensaas, L., Arntsen, B., Hanken, N.-M., Basire, C., & Graue, K. (2011). 1000 m long gas blow-out pipes. *Marine and Petroleum Geology, 28*(5), 1047-1060. doi:http://dx.doi.org/10.1016/j.marpetgeo.2010.10.001

Marfurt, K. J., Scheet, R. M., Sharp, J. A., & Harper, M. G. (1998). Suppression of the acquisition footprint for seismic sequence attribute mapping. *Geophysics, 63*(3), 1024-1035.

Martinsen, O., & Nøttvedt, A. (2008). *The making of a land - geology of Norway* (I. B. Ramberg, I. Bryhni, A. Nøttvedt, & K. Rangnes Eds.). Trondheim: Norges Geologiske Forening

McKerrow, W. S., Mac Niocaill, C., & Dewey, J. F. (2000). The Caledonian Orogeny Redefined. *Journal of the Geological Society, 157*, 1149-1154.

Moore, W. S., & Wilson, A. M. (2005). Advective flow through the upper continental shelf driven by storms, buoyancy, and submarine groundwater discharge. *Earth and Planetary Science Letters, 235*(3–4), 564-576. doi:http://dx.doi.org/10.1016/j.epsl.2005.04.043

Nichols, G. (2009). *Sedimentology and Stratigraphy* (Second ed.). United Kingdom: John Wiley & Sons

NORLEX. Barents Sea Chart. Retrieved from http://nhm2.uio.no/norges/litho/Barents_Chart.html

NPD. Snøhvit factpage. Retrieved from http://factpages.npd.no/FactPages/default.aspx?nav1=field&nav2=PageView|All&nav3=2053062

NPD. (2013). *Petroleum Resources on the Norwegian Continental Shelf, Exploration* (978-82-7257-103-9). Retrieved from Stavanger:

References.

NPD. (2016a). Factpage wellbore 7119/9-1. Retrieved from http://factpages.npd.no/FactPages/Default.aspx?nav1=wellbore&nav2=PageView|Exploration|All&nav3=132&culture=en

NPD. (2016b). Factpage wellbore 7119/12-1. Retrieved from http://factpages.npd.no/FactPages/Default.aspx?nav1=wellbore&nav2=PageView|Exploration|All&nav3=121&culture=en

NPD. (2016c). Factpage wellbore 7119/12-2. Retrieved from http://factpages.npd.no/FactPages/Default.aspx?nav1=wellbore&nav2=PageView|Exploration|All&nav3=114&culture=en

NPD. (2016d). Factpage wellbore 7119/12-3. Retrieved from http://factpages.npd.no/FactPages/Default.aspx?nav1=wellbore&nav2=PageView|Exploration|All&nav3=17&culture=en

NPD. (2016e). Factpage wellbore 7119/12-4. Retrieved from http://factpages.npd.no/FactPages/Default.aspx?nav1=wellbore&nav2=PageView|Exploration|All&nav3=6468&culture=en

NPD. (2016f). General Information, survey stp0825. Retrieved from http://factpages.npd.no/FactPages/default.aspx?nav1=survey&nav2=PageView|Finished|2008&nav3=4613&culture=en

Ostanin, I., Anka, Z., di Primio, R., & Bernal, A. (2012). Identification of a large Upper Cretaceous polygonal fault network in the Hammerfest basin: Implications on the reactivation of regional faulting and gas leakage dynamics, SW Barents Sea. *Marine Geology, 332–334*, 109-125. doi:http://dx.doi.org/10.1016/j.margeo.2012.03.005

Plaza-Faverola, A., Bünz, S., & Mienert, J. (2011). Repeated fluid expulsion through sub-seabed chimneys offshore Norway in response to glacial cycles. *Earth and Planetary Science Letters, 305*(3-4), 297-308. doi:10.1016/j.epsl.2011.03.001

Plaza-Faverola, A., Bünz, S., & Mienert, J. (2012). The free gas zone beneath gas hydrate bearing sediments and its link to fluid flow: 3-D seismic imaging offshore mid-Norway. *Marine Geology, 291-294*, 211-226. doi:10.1016/j.margeo.2011.07.002

Rajan, A., Bünz, S., Mienert, J., & Smith, A. J. (2013). Gas hydrate systems in petroleum provinces of the SW-Barents Sea. *Marine and Petroleum Geology, 46*, 92-106. doi:http://dx.doi.org/10.1016/j.marpetgeo.2013.06.009

Rider, M. K., Martin. (2011). *The Geological Intrepretation of Well Logs* (3 ed.). Glasgow: Rider-French Consulting Ltd

Rise, L., Bellec, V., Chand, S., & Bøe, R. (2015). Pockmarks in the southwestern Barents Sea and Finnmark Fjords. *Norwegian Journal of Geology, 94*, 263-282.

Schlumberger. (2014). Petrel E&P Software Platform 2014: Schlumberger. Retrieved from https://www.software.slb.com/products/petrel

Torsvik, T. H., Carlos, D., Mosar, J., Cocks, L. R. M., & Malme, T. (2002). Global reconstructions and North Atlantic paleogeography 440 Ma to Recent In E. Eide, A. (Ed.), *BATLAS - Mid Norway plate reconstruction atlas with global and Atlantic perspectives* (pp. 18-39). Trondheim: Norges Geologiske Undersøkelse.8273851060

Vadakkepuliyambatta, S., Bünz, S., Mienert, J., & Chand, S. (2013). Distribution of subsurface fluid-flow systems in the SW Barents Sea. *Marine and Petroleum Geology, 43*, 208-221. doi:http://dx.doi.org/10.1016/j.marpetgeo.2013.02.007

References.

Vadakkepuliyambatta, S., Hornbach, M. J., Bünz, S., & Phrampus, B. J. (2015). Controls on gas hydrate system evolution in a region of active fluid flow in the SW Barents Sea. *Marine and Petroleum Geology, 66, Part 4*, 861-872. doi:http://dx.doi.org/10.1016/j.marpetgeo.2015.07.023

Vincent, K. K., Muthama, M. N., & Muoki, S. N. (2014). Darcy¡¯s Law Equation with Application to Underground Seepage in Earth Dams in Calculation of the Amount of Seepage. *American Journal of Applied Mathematics and Statistics, 2*(3), 143-149.

Watterson, J., Walsh, J., Nicol, A., Nell, P. A. R., & P.G., B. (2000). Geometry and origin of a polygonal fault system. *Journal of Geological Society, 157*, 151-162.

Wille, P. C. (2005). *Sound Images of the Ocean in Research and Monitoring*. Berlin, Germany: Springer-Verlag Berlin Heidelberg

Winsborrow, M. C. M., Andreassen, K., Corner, G. D., & Laberg, J. S. (2010). Deglaciation of a marine-based ice sheet: Late Weichselian palaeo-ice dynamics and retreat in the southern Barents Sea reconstructed from onshore and offshore glacial geomorphology. *Quaternary Science Reviews, 29*(3-4), 424-442. doi:10.1016/j.quascirev.2009.10.001

8 Appendix.

8.1 Stratigraphy Chart – Geological Time.

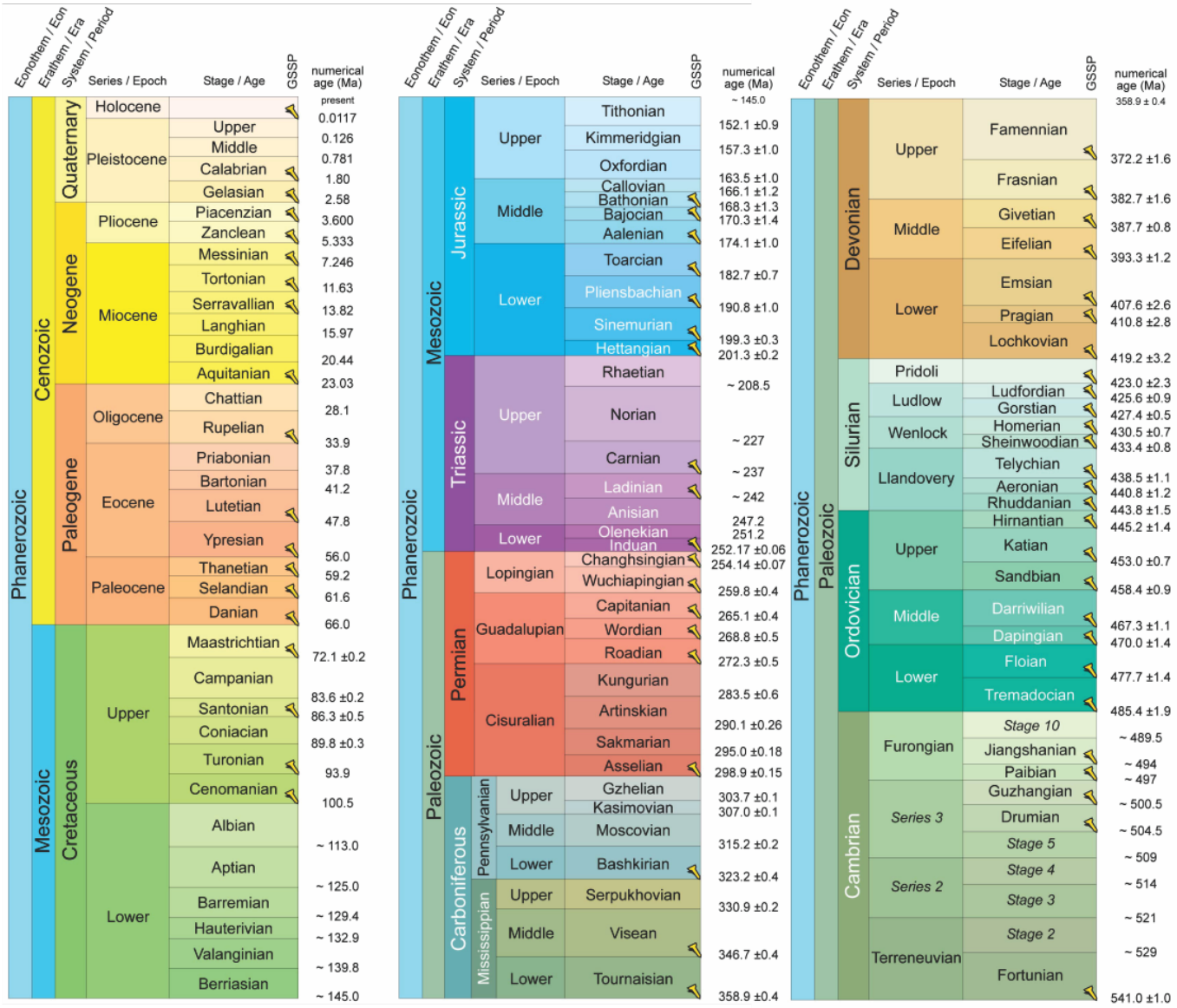

Fig. 30 The International Stratigraphy Chart v2015/01 Modified from Cohen et al. 2013.